Environmental Science and Pollution Research (2022) 29:55367–55399
https://doi.org/10.1007/s11356-022-21079-z

REVIEW ARTICLE

Stainless steel catalyst for air pollution control: structure, properties, and activity

Weixiao Wang[1] · Shunzheng Zhao[1,2] · Xiaolong Tang[1,2] · Chaoqi Chen[1] · Honghong Yi[1,2]

Received: 17 March 2022 / Accepted: 21 May 2022 / Published online: 7 June 2022

Abstract

With the awakening of environmental awareness, the importance of air quality to human health and the proper functioning of social mechanisms is becoming increasingly prominent. The low cost and high efficiency of catalytic technique makes it a natural choice for achieving deep air purification. Stainless steel alloys have demonstrated their full potential for application in a variety of catalytic fields. The diversity of 3D networks or fibrous structures increases the turbulence within the heterogeneous catalysis, balance the temperature distribution in the reaction bed and, in combination with a highly thermally conductive skeleton, avoid agglomeration and deactivation of the active components; corrosion resistance and thermal stability are adapted to highly endothermic/exothermic or corrosive reaction environments; oxide layers formed by bulk transition metals activated by thermal treatment or etching can significantly alter the physico-chemical properties between the substrate and active species, further improving the stability of stainless steel catalysts; suitable electronic conductivity can be applied to the electrothermal catalysis, which is expected to provide guidance for the reduction of intermittent emission exhausts and the storage of renewable energy. The current applications of stainless steel as catalyst or support in the air purification have covered soot particle capture and combustion, catalytic oxidation of VOCs, SCR, and air sterilization. This paper summarizes several preparation methods and presents the relationships between the preparation process and the activity, and reviews its application and the current status of research in atmospheric environmental management, proposing the advantages and challenges of the stainless steel-based catalysts.

Keywords Stainless steel · Metal monolith catalysts · Air pollution control · VOCs · SCR · Soot

Introduction

According to the United Nations Environment Programme UNEP (2021), by 2020, more than 95% of countries are regulating PM_{10}, ozone, nitrogen oxide (NOx) and sulfur dioxide (SO_2), and 90% are regulating $PM_{2.5}$. But due to cost or technical constraints, few standards are as stringent as the WHO Air Quality Guidelines (AQGs 2005) (Health Effects Institute 2020). This indicates that air quality control will be a hotspot for a long time in the future. However, with the deepening of the pollution control process, the space for pollutant reduction is gradually narrowing, and it is becoming increasingly difficult to reduce emissions from end-of-pipe treatment (Aljerf 2016).

Among the pollution control technologies that have been developed, catalysis (including catalytic oxidation and catalytic reduction) is widely used, energy-saving, and free of secondary pollution. It has a great potential for emission reduction, which makes them an inevitable choice for in-depth air environmental control worldwide.

The research and development of catalysts are one of the cores of catalytic technology. Structured catalysts and reactors have gained a lot of attention because they show more freedom in design than filled-bed ones, which have the drawbacks of high pressure drop, hard separation and ineffective recovery (Rogozhnikov et al. 2022). A typical case

Responsible Editor: George Z. Kyzas

Weixiao Wang and Shunzheng Zhao contributed equally to this work.

✉ Honghong Yi
yhhtxl@163.com

[1] School of Energy and Environmental Engineering, University of Science and Technology Beijing, Beijing 100083, China

[2] Beijing Key Laboratory of Resource-Oriented Treatment of Industrial Pollutants, Beijing 100083, China

of this type of catalyst is the monolithic catalyst, which is mostly in the form of a honeycomb or layer structure, usually made of ceramics or metals (Carty & Lednor 1996; Bao and Wu 2022). Ceramic Honeycomb (CH) has become one of the most important and promising supports due to its low thermal expansion and high thermal shock fracture resistance (Hu and Wang 2021). However, it suffers from fragility, lack of alkali resistance and poor thermal conductivity (Liu et al. 2017); On account of process limitations, the walls of CH are usually thick and closed, inhibiting radial mixing of the gas stream and leading to poor interphase mass transfer rates (Yao et al. 2020); While low thermal conductivity and mixing degree of airflow further result in low heat transfer rates and uneven temperature distribution in catalytic bed, especially in highly exothermic and endothermic reactions, where local hot spots are inevitable due to the occurrence of laminar phenomena, which gives rise to catalyst agglomeration and inactivation (Yao et al. 2022). Secondly, for CH catalysts, the introduction of the active component is usually incorporated into the channel walls during the structure forming stage or coated by washing-coat, which generates poor exposure of the active sites or accumulation of coating at the corners (Yao et al. 2006). Most importantly, for dusty gases (e.g., coal-fired boiler tail gas), once the front channels of the catalyst are blocked by dust, the entire catalyst will fail completely, leading to frequent disassembly and installation of the system and high operating and maintenance costs.

In contrast, metallic supports offer significant advantages. First, the metal substrate is more suitable for the harsh atmosphere of highly exothermic and endothermic reactions as its better thermal conductivity, lower heat capacity, greater resistance to thermal and mechanical shock (Chen et al. 2019). Secondly, it also tends to have thinner walls and larger free cross-section, resulting in lower pressure drop and greater contact area per unit volume for the same pore density, thus enabling higher conversion efficiencies (Wu et al. 2005; Kucharczyk et al. 2017). Thirdly, metal blocks are easy for remoulding and can be adapted to different geometries required in various industrial applications (Banus et al. 2014; Godoy et al. 2018), improving the mass transfer capability of the catalyst. In addition, when a metal-based catalyst with suitable resistivity is selected, it can act as a resistive element for joule-heating of the reaction system (Duran et al. 2011). Therefore, metal supports have received increasing attention.

Currently, the commonly used metal supports are Fe (Xue et al. 2020), Al (Agueniou et al. 2020; Xia et al. 2020), Ni (Agueniou et al. 2020; Bello et al. 2013; Zha et al. 2020; Zhao et al. 2020), Cu (Agueniou et al. 2020), Ni–Cr alloys (Nady et al. 2021; Zhou et al. 2008), etc. Among these, stainless steel (SS) is regarded as a good candidate due to its availability, low cost and the presence of numerous transition metal elements (Fe, Ni, and Cr, etc.) (Anantharaj et al. 2017). It has been well documented that SS has good electronic conductivity and corrosion resistance in complex catalytic environments (Schafer and Chatenet 2018). Its chemical properties and catalytic behaviour can be regulated by surface modification. For example, acid leaching increases the surface area (Schafer and Chatenet 2018; Shen et al. 2018), surface elements modulating to obtain better catalytic activity (Lee et al. 2018). Therefore, in recent years, stainless steel monolithic catalysts have been widely used in a variety of catalytic fields, such as pollutant abatement (Godoy et al. 2018; Sanz et al. 2017; Yang et al. 2006), organic synthesis (Chang et al. 2021), clean energy (Huang et al. 2021; Liu et al. 2021; Zhu et al. 2019a).

Although a large number of articles have studied or summarized the preparation and related applications of metal-based monolithic catalysts (Montebelli et al. 2014; Pauletto et al. 2020), there are no reports that focus exclusively on stainless steel substrates, and the applications covered in the above articles are mostly broad, including purification of different environmental media, chemical synthesis, electrochemical cells and reforming reaction, etc. It is therefore of great significance to narrow down the scope of research for better understanding the catalytic performance of stainless steel and promoting the further purification of the atmospheric environment. In addition, inspired by the element-rich property of stainless steel, some novel preparation methods (e.g. etching, thermal treatment) have been developed to activate its inert surfaces. These methods improve surface roughness of SS, exploit its potential catalytic activity and/or enhance substrate-active component interactions, which altering the valence state of surface elements or even the active site. Based on this, this paper summarises the advantages and challenges of stainless steel as a catalyst or support from the perspective of air pollution control; outlines the preparation methods, including the synthesis of coatings and the deposition of active phase; and reviews their application and research status in different fields, aiming to provide a basis for the promotion and development of stainless steel in catalysis.

Properties of stainless steel-based catalysts

Physical properties

When describing the properties of stainless steel, corrosion resistance, hardness, strength, toughness, density, magnetism, etc. are the most important index. But in this paper, only properties closely related to catalysis are introduced, such as resistivity, thermal expansivity, and thermal conductivity (see Table 1).

Stability is a critical factor in support selection. The working temperature window for the catalytic combustion

Table 1 Physical properties of stainless steel related to catalysis

Type	Resistivity / (μΩ·cm)	thermal expansivity / ($\times 10^{-6}$ K^{-1})	Thermal conductivity /($W{\cdot}m^{-1}{\cdot}K^{-1}$)	Maximum service temperature in air / (℃)
AISI301	70–72	18.0	16.3	-
AISI302	70–72	15–18	16.3	-
AISI304	70–72	18.0	16.3	-
AISI310	70–78	16–18	16.3	-
AISI316	70–78	16–18	16.3	-
AISI321	70–73	18.0	16.3	800
AISI347	70–73	16–18	16.3	800
AISI410	56–72	10–12	18–24	750
AISI420	55	10.3	24.9	-

of air pollutants is generally between 200 ~ 500 ℃, well below the temperature limit (~ 800 °C) of stainless steel in the air (the ambient atmosphere for most catalytic reactions) (du Preez et al. 2019). On the other hand, good acid and alkali resistance are also major reasons for the popularity of stainless steel catalysts.

For gas–solid heterogeneous catalytic systems, the hazards of localised overheating of the active center have been well documented (Badmaev and Sobyanin 2020). Sanz et al. (2016) pointed out that the lower the thermal conductivity the more significant the temperature difference in the catalytic bed and the more pronounced the local hot spot. The excellent thermal conductivity of stainless steel has become an important factor in its widespread use as catalyst support. As shown in Fig. 1a, both axial and radial temperature gradients within the catalyst module are negligible during a strongly endothermic reaction (Zazhigalov et al. 2021). However, in addition to its intrinsic thermal conductivity, the actual thermal conductivity is also related to the pore density of the substrate, that is, the number of pores per unit cross-sectional area. Visconti et al. (2013) have proved that the higher the pore density, the higher the thermal conductivity in the axial and radial directions.

In line with transition state theory, any reaction must cross an energy barrier before it can be converted to a product. Therefore, extra energy is needed to input to the system to bring the ambient temperature to the catalyst's ignition temperature. The traditional external heating model leads to large equipment volume and high operating costs, and inevitably produces a great heat loss. In this situation, making full use of the resistance element as catalyst supports for the self-heating of the system has emerged. Stainless steel meets the resistance requirements for joule-heating and is a cheap alternative to the traditional FeCrAl wire.

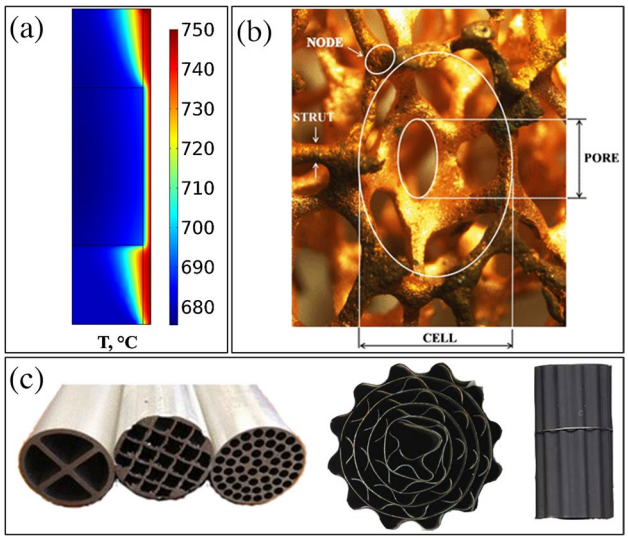

Fig. 1 (**a**) Temperature distribution along the stainless steel wire mesh honeycomb module in endothermic reaction (furnace T = 750 ℃) (Zazhigalov et al. 2021). (**b**) Open-cell foam geometrical characterization (Montebelli et al. 2014). (**c**) Different forms of WH: Columnar monolith (left) (Montebelli et al. 2014) and spiral roller (right) (Martinez et al. 2009)

Structural properties

The plasticity of stainless steel enables it to be adapted to different processes and thus to be used in different geometrical forms (like wire, foil, plate, tube, foam, honeycomb, wire mesh, fibre felt, etc.), as shown in Fig. 2.

Metallic foams (MF) are bulk materials with continuous cellular network structure. As shown in Fig. 1b, the unit cell structure of MF is usually a polyhedron, its pore density is evaluated by the number of pores per linear inch (PPI). PPI of typical MF is 5 ~ 40, and the void ratio is 90 ~ 95% (Montebelli et al. 2014), which has a high surface area to volume ratio. Compared with honeycomb, metal foams can obtain a wider range of shapes and have shorter diffusion distances.

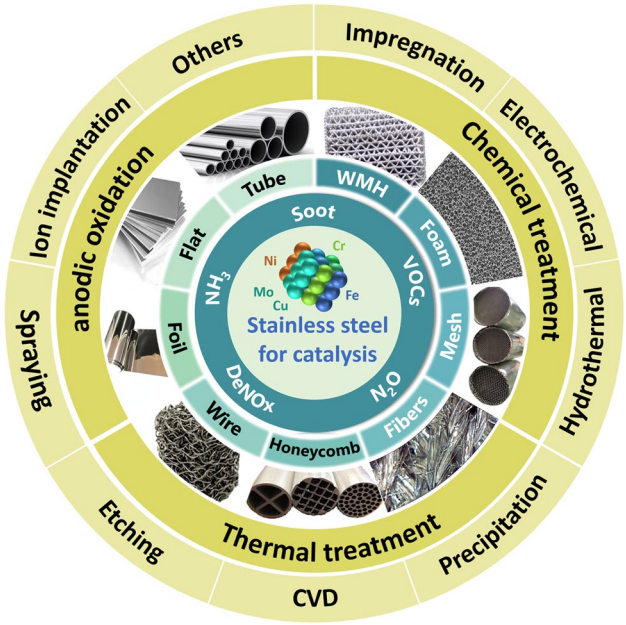

Fig. 2 Geometrical structure, preparation, and application of stainless steel catalysts

In addition, the zigzag pore shape facilitates reactants mixing and external mass transfer, allowing radial mass and heat transfer. In some cases, the interconnect network makes the radial heat transfer of metal foam superior to that of metal honeycomb. Compared to other forms of metal supports, metal foams achieve better adhesion of the catalytic layer.

Metal honeycomb (MH) is made by extruding or rolling corrugated plates and flat foils in turn. The general structure parameter is CPSI, the number of cells per square inch. In general, the pore densities of MH vary from 50 to 600 CPSI and the void ratio is usually in the range of 70 ~ 90% (Montebelli et al. 2014). The closed, parallel channel walls allow for a straight, vortex-free fluid path. By contrast, the rolling method produces a more flexible geometry, commonly in the form of columnar monoliths or spiral rollers (Fig. 1c). However, the disadvantage of this method is that the continuity of the material is sacrificed, resulting in a poor effective radial thermal conductivity (even after welding).

Wire Mesh (WM) is a combination of multiple layers of mesh. Porsin et al. (2016) pointed out that with the same loading of active components, WM catalyst has better flame-out performance than MH catalyst, this is because the mesh structure avoids the formation of laminar flow of gases, thus providing higher mass and heat transfer efficiency and eliminating the limitation of external diffusion (e.g. pore diffusion and axial diffusion). It is suitable for flue gas purification and high space velocity reactions. Its best-known application relates to nitric acid production, a process with air velocity of up to 600,000 h^{-1}. Additionally, the structure design has high flexibility, allowing the size, shape, wire diameter, and packing density of the mesh to be varied to control the reaction environment parameters (e.g. pressure drop, mass and heat transfer rates, etc.). These advantages allow the creation of compact and efficient catalytic reactors with heating surfaces of varying shapes, but with the problem of cumbersome assembly.

Table 2 Physical properties of WMH and CH catalysts (Qu et al. 2013; Shu et al. 2012a)

Sample	WMH	CH
Materials	Stainless steel	Cordierite
Cell shape	Sine wave	Square
Cell density/(cpsi)	100	100
GSA/($\times 10^3$ $m^2 \cdot m^{-3}$)	1.62	1.28
OFA/(%)	74.1	64.3
Dh/($\times 10^{-3}$ m)	2.54	2.03
Pressure drop/(10^{-2} Pa)	2.58	5.08

GSA geometric surface area, *OFA* open frontal area, *Dh* hydraulic diameter.

Wire mesh honeycomb (WMH) is a modification of WM, which is rolled by corrugated mesh or stacked alternately with flat ones. The channel walls are interconnected to form a three-dimensional opening structure. Table 2 shows a comparison of the geometric properties of WMH and CH for the same pore density (Qu et al. 2013; Shu et al. 2012a). It can be found that the WMH catalyst offered higher geometric surface area (GSA), open frontal area (OFA) and large hydraulic diameter (Dh) than the CH catalyst, which could help to minimize the pressure drop and increases the interphase mass transfer rate and resistance to dust accumulation, and avoids the accumulation of the active coating at the corners (Yao et al. 2006), maximizing the utilization of the catalyst per geometric area (Shu et al. 2012b).

For WM and WMH catalysts, the uniform distribution of temperature is also associated with the presence of gas radial mixing. This conferred a faster thermal (Fig. 3a) and reactant response (Fig. 3b) to the catalysts (Qu et al. 2013; Sanz et al. 2016). All catalysts heated up within 5 min and remained at this temperature for 50 min. It can be seen that the WMH catalysts took half the time to achieve activity stabilization compared to the CH catalysts, taking only 10 min, and achieved higher product conversions at the same temperature. In the reactant response experiment, when reactants were abruptly cut off or supplied, the WMH catalyst reached steady-state conversion in a shorter time.

Loosely joined wires or fibers in a geometrically interlaced pattern called metal fibre felt (Fibers). The open and porous nature of this material provides a high degree of gas turbulence and gas–solid contact area, thus possess higher adsorption properties and catalytic activity towards gaseous pollutants. Yin et al. (2019) found that

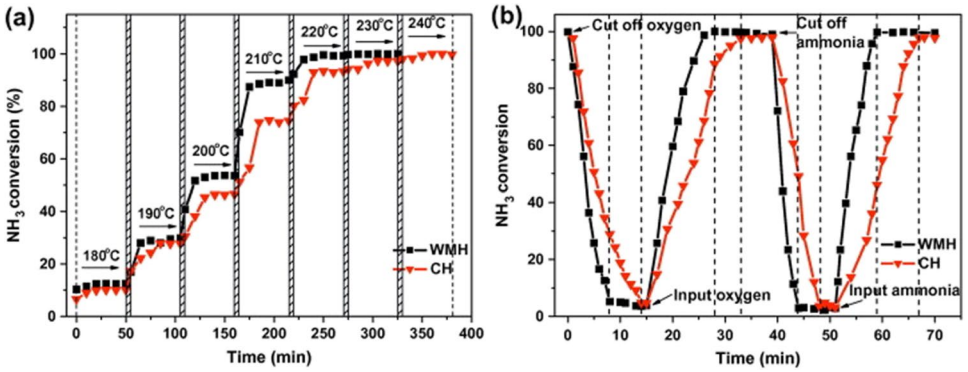

Fig. 3 Thermal response (**a**) and reactant response (**b**) over WMH and CH catalysts (Qu et al. 2013)

ZIF-67 membrane supported on paper-like stainless steel fibers (PSSF) displayed higher adsorption rate constant of toluene (0.0672 min^{-1}) than granular ZSM-5 zeolites (0.0560 min^{-1}), which is closely related to the higher mass transfer efficacy offered by the three-dimensional network structure of PSSF. For this reason, metal fibers have been extensively investigated in the fields of gas-phase synthesis (Pauletto et al. 2021a, 2021b; Qu et al. 2013), contaminant purification (Chen et al. 2022b; Zhou et al. 2017).

Although different structures and geometries of stainless steel have been developed, mesh and honeycomb are the most widely used, taking into account the ease of construction and shape advantages.

Chemical properties

According to the definition of GB/T20878-2007, the main component of stainless steel is Cr (≥ 10.5%). This is the main contributor to its rust resistance. Other elements in SS also include Mn, Ni, Mo, Cu, Si, Nb, N, etc., to meet the requirements of stainless steel structure and performance for various applications.

Studies have shown that the presence of transition metal elements (Fe, Ni, Mn, Cr, Cu) in stainless steel endows its certain catalytic activity, and only requires appropriate treatment to activate the surface (such as calcination, surface etching) (Huang et al. 2021; Liu et al. 2021). Duran et al. (2011) used AISI 304 roasted at 900 °C in an air flow for 2 h for the catalytic oxidation of ethyl acetate. The results showed that the transformation of ethyl acetate was complete below 400 ℃, T_{80} = 370 ℃. Xin et al. (2019) synthesized Carbon nanosprouts (CNS) by using calcined SS as the catalyst. The FeO nanoparticles formed by calcination were the main catalytic active phase, while the presence of Mn also promotes the synthesis of CNS, as shown in Fig. 4. Similarly, Baddour et al. (2009) found that SS matrix etched by HCl (such as plates, wire meshes and powders) could also achieve the gas-phase synthesis of MWCNTS without addition of any catalyst. du Preez et al. (2019) prepared a Pt-loaded stainless steel mesh and found that Ni in SS promoted catalytic hydrogen combustion. Chen et al. (2019) performed

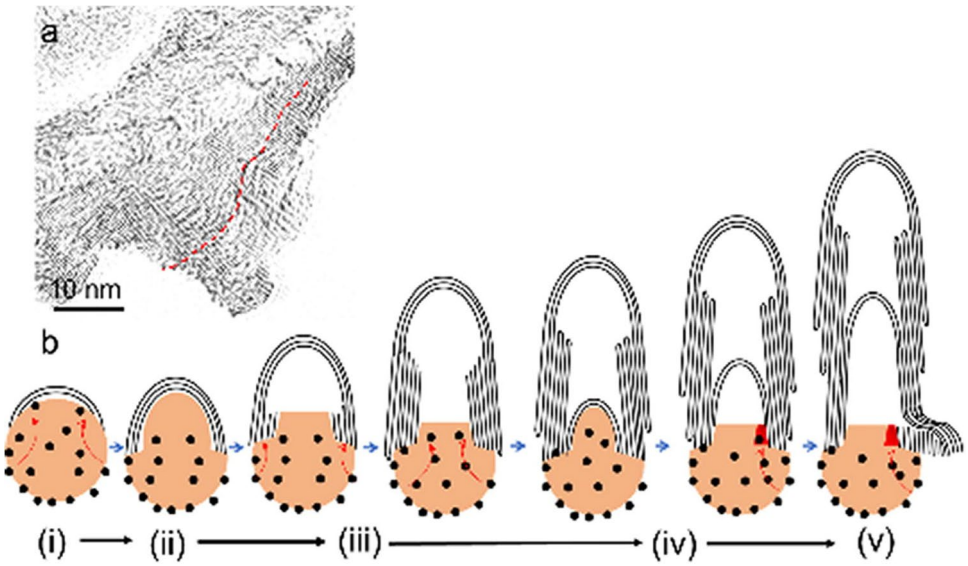

Fig. 4 TEM image of a nanosprout (**a**) and schematic illustration of carbon nanosprout formation process (**b**) (Xin et al. 2019)

a one-step hydrothermal synthesis on AISI304 wire mesh to obtain a series of Mn-based monolithic catalysts. The results showed that during the hydrothermal and calcination process, Cr and Fe in the wire mesh doped into the MnO_2 matrix, creating oxygen vacancies, increasing lattice stress and greatly improving the catalytic performance.

However, given that the inherent catalytic activity of stainless steel substrates is not sufficient to meet practical demands, it is essential to develop different preparation methods to enable the large-scale production and application of stainless steel supported catalysts.

Preparation of stainless steel catalyst

The preparation of the structured catalyst is crucial to the properties (activity, mechanical properties, etc.) that the catalyst will ultimately exhibit. Unlike the possibility of direct extrusion of the ceramic catalyst, the metal support has to be additionally loaded with catalytic layers. It is accepted that the adhesion of inorganic coatings on metals is more difficult than on ceramics (Aljerf 2015). This is because the smooth, chemically inert surface of the metals, its low specific surface area and the large difference in thermal expansivity between it and the oxide coating or active phase film, leading to creeping and flaking of the catalytic film during subsequent preparation and service. In addition, under high temperature conditions, some active components may migrate into the substrate by thermal diffusion. At the same time, oxygen will also pass through the catalyst coating to contact the substrate, resulting in the oxidation of the metal surface (Wu et al. 2001). This seriously affects the lifetime and stability of metal-based monolithic catalysts. Therefore, the primary problem of preparing metal-based catalysts is to solve the adhesion of the catalytic layer (oxide carrier + active phase) (Banus et al. 2010).

A summary of the published literature shows that the preparation of metal-based catalysts mostly includes the following steps: 1) surface pretreatment; 2) coating of the intermediate coating and 3) loading of the active phase. Surface pre-treatment of the metal substrate improves the surface roughness, promotes the formation of porous oxide layers and ensures good adhesion of the intermediate coating and the active phase. The intermediate coating is present to further increase the surface area of the catalyst to expose more active sites. The loading of the active phase is a key step in acquisition of catalytic activity. Most of the time, these three steps are not completely hierarchical and independent. In other words, once the oxide film produced by the pretreatment has reached a suitable thickness and adhesion, the preparation of the intermediate coating can be dispensed with and the loading of the active component can be carried out directly. Alternatively, the active phase can be incorporated into the intermediate coating precursor to simplify the preparation process.

In general definitions, coatings refer to secondary supports and/or active phase films, as shown in Fig. 5a. Montebelli et al. (Montebelli et al. 2014) classified the coatings into three categories according to their functions and processes: 1) Morphological supports: regulating the surface topography of substrate, and active phases need to be further deposited; 2) direct deposition of ready-made catalysts; 3) in-situ growth of active phase. This section provides a brief overview of surface pre-treatment and catalytic layer coating techniques for metal substrates (Fig. 5b).

Pretreatment

Chemical treatment

Chemical treatment is the first step in the pretreatment of metal substrates, mostly using organic solvents such as ethanol and/or acetone for ultrasonic cleaning, with the aim of removing grease and dust that may exist on the surface of the substrate. In other studies, strong acid (HCl, HNO_3) or base (NaOH) was subsequently used for corrosion treatment to increase surface roughness and promote the formation of the oxide layer. Suknev et al. (2004) state that HCl treatment helps to form a pseudo-layer that facilitates the chemisorption of small charged particles.

Thermal treatment

During the preparation and use of catalysts, high-temperature conditions can cause some components in stainless steel to migrate from bulk phase to surface, and these segregated metals can interact with the catalytic phase and thus alter the catalytic activity. Calcination of stainless steel at high temperature can induce metal migration beforehand, generating an oxide layer to avoid further metal segregation in subsequent sections. The generated oxide layer can also improve the roughness of the metal substrate surface and increase the surface area, ensuring good adhesion of the active components and uniform distribution of the active metal (Banus et al. 2010; Bortolozzi et al. 2010; Chen et al. 2019). In turn, the porosity of the oxide layer also allows the transport of gaseous oxygen, improving the mass transfer efficiency in heterogeneous catalytic systems (Saeki et al. 1998).

The metal oxide coating formed by calcination depends on the composition of the metal substrate. Karimi et al. (2008) proposed the oxidation layer growth mechanism of AISI 304 in the air at 1000 ℃. At the initial stage of oxidation, the oxide layer grows outwards and consists of $Mn_{1.5}Cr_{1.5}O_4$ and Cr_2O_3. The metal substrate exhibits Cr depletion near the interface. In the second step, Fe diffuses outwards through the initially formed oxide layer and Cr_2O_3

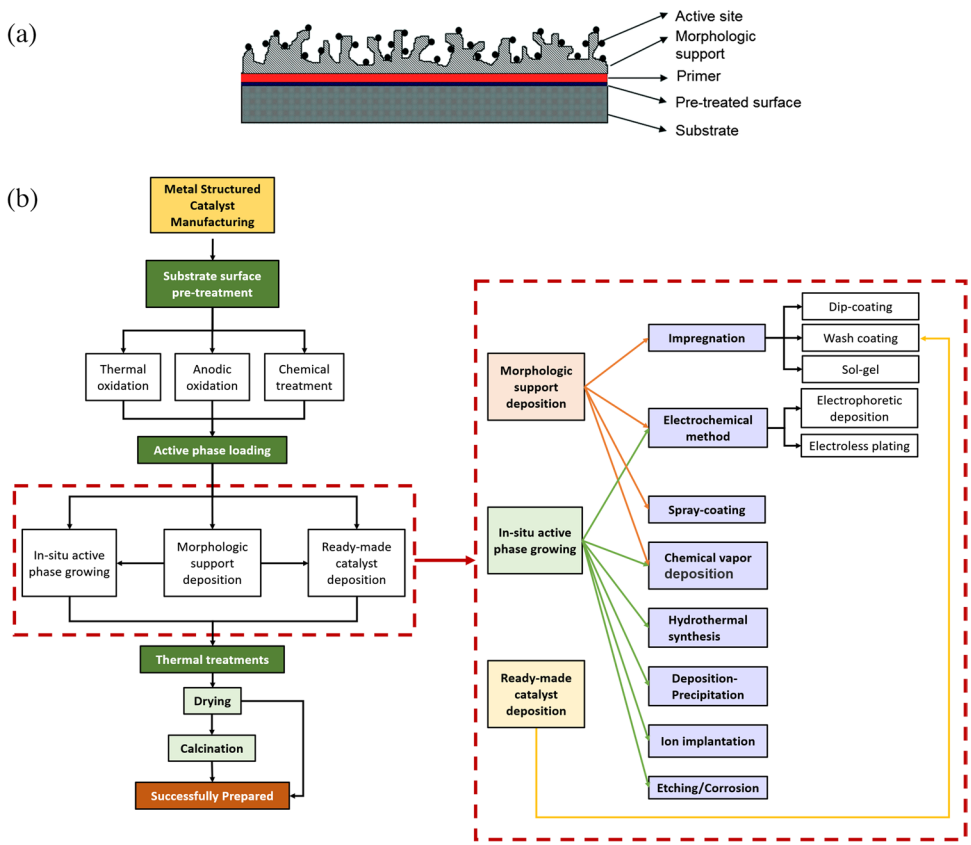

Fig. 5 Sketch of structured catalyst (**a**), and main steps involved in the preparation of a metallic structured catalyst (**b**)

is converted mainly to $FeCr_2O_4$. At the same time, Fe_2O_3 was formed at the air/oxide interface. This process results in an iron depletion at the rust layer and stainless steel surface, where the main element becomes Ni and holes are formed at the interface. After a certain period of oxidation, iron no longer diffuses outwards through the external oxide layer. This is related to the fact that the outer sub-rust layer is no longer in contact with the metal substrate.

The selection of calcination parameters also influences the oxidation of stainless steel. Saeki et al. (1998) reported the effect of atmosphere on the oxidation of AISI 430 at 1000 ℃. 430 stainless steel contains relatively high manganese content. Under 1000 ℃ and $O_2/H_2O/N_2$ atmosphere, only an iron-rich corundum-type oxide was formed on the surface during the initial 15 s. Afterwards, with increasing oxidation time, Mn_2O_3 was reduced or decomposed into MnO and formed $MnFe_2O_4$ or $MnCrO_4$ spinel-type oxides by solid-state reaction with Fe_2O_3 or Cr_2O_3. Of these, the phase is rich in Cr at higher oxygen partial pressures and Fe at lower oxygen partial pressures. Duran et al. (2011) found that the oxidation rate of AISI 304 was faster and the stability of the oxide layer was better in an airstream compared to a static atmosphere. It was suggested that when the particle spacing in the oxide layer is about 2/3 of the catalyst particle diameter, it was more favorable to physically anchor the active component. Bortolozzi et al. (2010) studied the influence of calcination temperature and time on the surface chemistry and morphology of the AISI 314 foam. The results show that Cr_2O_3, Fe_2O_3, $Mn_{1+X}Cr_{1-X}O_{4-x}$, $FeCr_2O_4$ spinel complex oxides, as well as a small amount of FeO and Fe_3O_4 are produced under high-temperature calcination. The effects of calcination temperature and time on sample weight, oxide layer thickness and oxide layer adhesion is shown in Table 3. It can be seen that an increase in temperature or time caused an increase in oxidation degree. The above phenomena indicate that the relative abundance of major elements in the oxide layer of stainless steel substrate can be controlled by adjusting parameters such as reaction temperature, time and oxidation atmosphere, which could promote the in-situ growth of active phase and/or improve the chemical affinity between catalyst and metal support (Duran et al. 2011). However, it should be noted that the high-temperature oxidation process will reduce the thermal and electrical properties of the materials (Montebelli et al. 2014), which does not facilitate the subsequent electrochemical deposition (Li et al. 2017a).

Compared to chemical treatment, heat treatment is more effective in improving the adhesion of the active phase (Padilha et al. 2006). This is mainly due to the fact that the oxide whiskers on the surface of the substrate after heat treatment not only increase the surface roughness, but also completely change the interfacial properties

Table 3 Effects of calcination temperature and time on sample weight, oxide layer thickness and adhesion of oxide layer (Duran et al. 2011)

Calcination parameters		Wight gain/(%)	Thickness/(um)	·Weight loss/(%)*
Time/(h)	Temperature/(℃)			
20	850	1.6	< 1	0.15
	900	2.5	1–1.5	0.10
	950	5	1–2	0.30
	1000	15.9	1.5–3	0.30
	1050	22.5	1.5–3	0.30
Temperature/(℃)	Time/(h)			
900	1	0.58	< 0.2	0.10
	2	0.85	0.7	0.10
	5	1.41	-	0.15
	10	2.09	0.9	0.20
	20	2.5	1–1.5	0.1

* The shedding rate of metal oxide layer under ultrasonic (40 kHz,160 W,60 min) test, which is measured by weight loss.

between the substrate and the active layer (active layer/oxide interface instead of active layer/metal interface), reducing the mechanical failure of the interface, see Fig. 6. In addition, it was shown that the combination of chemical treatment and heat treatment led to the formation of oxide whiskers on the corroded metal surface, thus

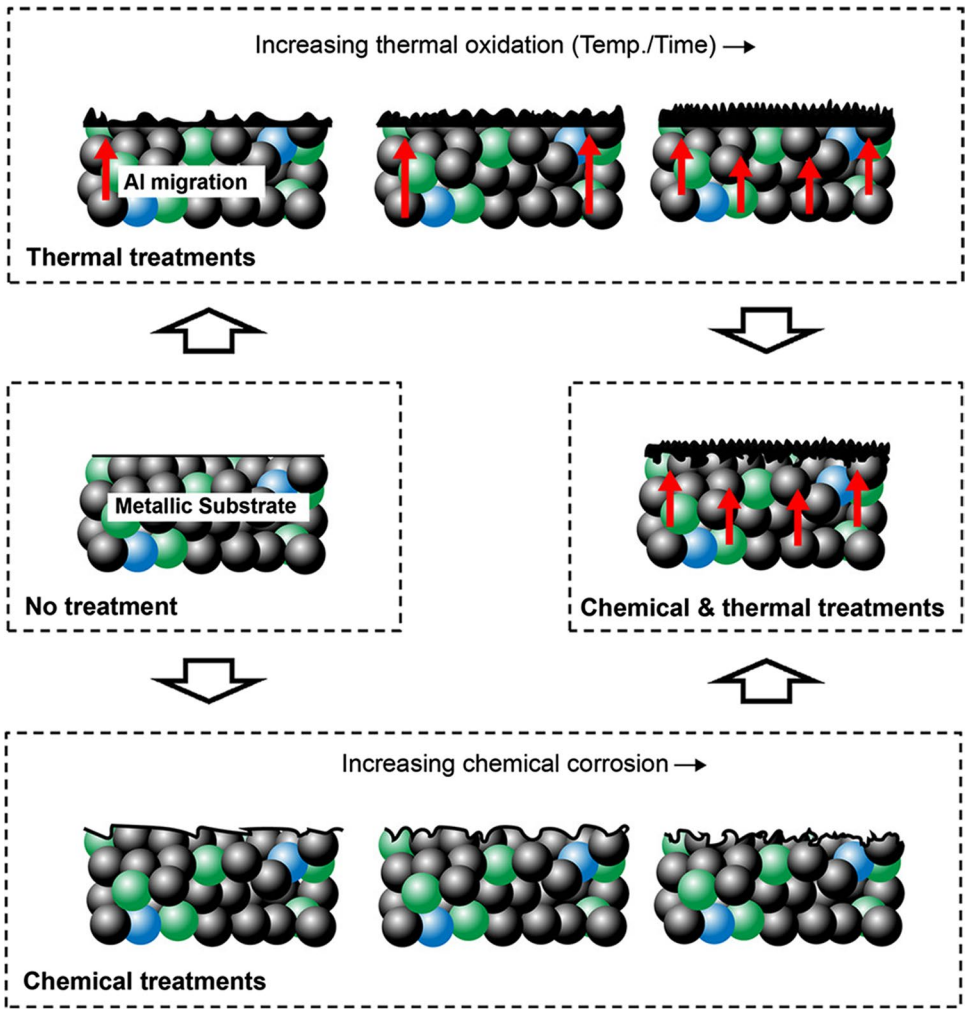

Fig. 6 Mechanism of the influence of the metallic substrate pretreatments on the washcoat adhesion (Pauletto et al. 2020)

giving the best anti-shedding performance of the active substance (Wu et al. 2017).

Anodic oxidation

Anodic oxidation is usually used for Al-containing substrates. The metal is dissolved under direct current (DC) and a porous layer of aluminium oxide is produced on its surface, thus promoting good dispersion of the active component on the support (Anonymous 1982).

Compared to calcination, anodic oxidation results in a much rougher and porous surface, while it takes less time and energy. Changes in the surface morphology of FeCrAl alloys after anodic oxidation and calcination were given by Li et al. (2017b). It can be seen that the calcination leads to protruded particles on the metal surface, while the anodized sample shows channels with diameter of 1 ~ 4 μm, which provide additional surface for the deposition of the catalytic phase (Fig. 7). Further impregnation of Al_2O_3 interlayer and MnOx revealed the coating integrity and the loading amount of Mn over anodized alloy are the best.

Anodic oxidation can be used either as a pre-treatment for another coating method or as a pre-coating prior to the loading of the active phase, i.e. impregnation was inflicted directly on the resulting porous layer to coating active components. The alumina layers obtained can be easily regulated by adjusting the anodic parameters, such as: electric potential, electrolyte (e.g. type and concentration) and temperature. Ganley et al. (2004) obtained the optimum porosity of Al_2O_3 under 0.6 mol/L oxalic acid, 18 ℃, and 30 V. The subsequent hydrothermal treatment further increases the surface area of the oxide layer to 25 m^2/g. Zhang et al. (2012) pointed out that the structure of anodic oxide film grown on SSWM with different electrolytes (acetic acid, oxalic acid, sulfuric acid solution) has a great difference. The textures of the SSWM treated by 5% acetic acid present the most pores.

However, along with these advantages, the anodic oxidation method is difficult to achieve mass production of catalysts, which makes its practical application difficult.

Loading of the active phase

In some cases, even if the metal surface has been pretreated according to the techniques described above, the stability of the catalyst cannot meet actual needs. It can be overcome by covering the substrate with an intermediate coating (typically Al_2O_3, SiO_2 or TiO_2). Generally speaking, the pre-coating and the catalytic layer are coated in much the same way and can be achieved by various methods, e.g., impregnation, electrodeposition, hydrothermal and so on. Therefore, this section introduces both together.

Impregnation

Impregnation is the most versatile and simple method for the preparation of catalysts, where the deposition of the active phase is achieved by submerging the substrate in a solution of the active precursors (Kotter et al. 1983). Of the

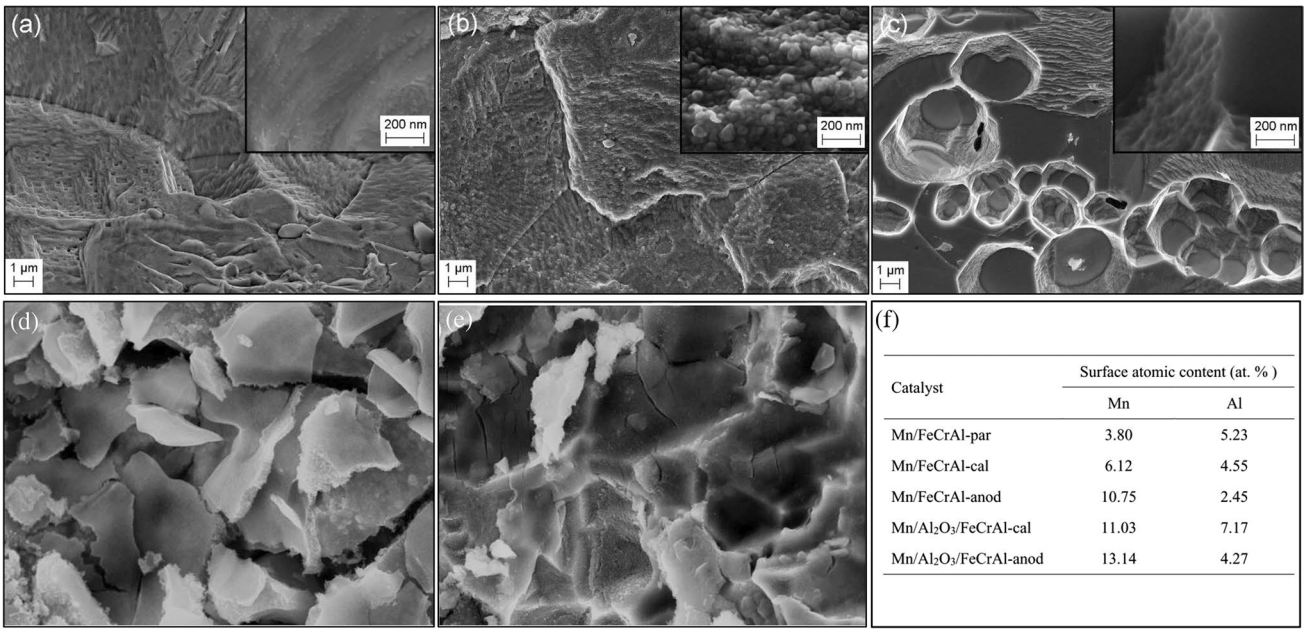

Catalyst	Surface atomic content (at. %)	
	Mn	Al
Mn/FeCrAl-par	3.80	5.23
Mn/FeCrAl-cal	6.12	4.55
Mn/FeCrAl-anod	10.75	2.45
Mn/Al_2O_3/FeCrAl-cal	11.03	7.17
Mn/Al_2O_3/FeCrAl-anod	13.14	4.27

Fig. 7 SEM images of the pristine (**a**), pretreated alloys (**b-c**) and the supported manganese oxide catalysts (**d-e**): FeCrAl-calcination (**b**, **d**), FeCrAl-anodized (**c,e**). Surface metal contents of the alloy-based catalysts (**f**) (Li et al, 2017b)

various impregnation techniques, sol–gel, dip-coating and wash-coating are the three most commonly used preparation methods. There are no clear boundaries between these three ways and the basic preparation steps can be divided into two steps: 1) impregnation of the structural substrate and 2) blowing off of the excess fluid (Fig. 8).

The starting point of the sol–gel method is a sol–gel dispersion of the coating precursor, which was initially used to prepare Al_2O_3 coatings and was then gradually extended to other coatings such as ZrO_2 (Yu et al. 2017), SiO_2 (Jeong et al. 2022), TiO_2 (Khan and Malik 2022), CeO_2 (Kavitha et al. 2022). An important factor in the process of sol–gel is the sol-gelation time. Depending on the concentration of the sol–gel and the characteristic size of support, the ageing time varies from a few minutes to several weeks, with the sol–gel viscosity being proportional to the ageing time (Alber and Cox 1997). However, it is worth noting that, catalysts prepared by the sol–gel have been found to have low catalytic activity usually due to the encapsulation of the active phase (Pecchi and Reyes 2003).

Dip-coating and wash-coating methods are not limited to colloidal dispersions, but can also be powder dispersions. But the precursors used in the wash-coating method contain a second support, that is, the active phase is first impregnated on an oxide powder with high specific surface area (such as γ-Al_2O_3 and CeO_2) (Govender and Friedrich 2017) to improve the distribution of the active component and avoid interaction with the surface of the metal substrate. The powdered catalyst is then formulated into slurries or sol–gel dispersions of suitable viscosity for the impregnation of the monolithic supports (Banus et al. 2010; Pauletto et al. 2020). To simplify the preparation process, the impregnating slurry can be prepared directly with ready-made powder catalysts.

Thickness, homogeneity and adhesion are three main design factors affecting the quality of impregnated coatings (Falsafein et al. 2018). Coating thickness depends heavily on slurry viscosity and the blowing-off process. The uniformity of coating is closely related to the stability of the slurry. pH, solids content, particle size and viscosity of slurry should be carefully controlled. ζ-potential is often used to determine the appropriate pH range. To avoid the agglomeration of particles, the absolute value of ζ should be greater than 20 mV (Santos et al. 2020). The settling property of the slurry is affected by solids content. The higher the solids content, the easier it is to settle, which leads to a large amount of adhesion but less homogeneous coating. The particle size of the active phase is negatively correlated with slurry viscosity. The higher the viscosity, the thicker the sediment, but the more prone to cracking (Meille 2006). In general, a viscosity of 7.5 mPa·s gives a suitable amount of coating without affecting the homogeneity of the catalytic layer. The adhesion of coating depends on the composition of the slurry and the porosity, packing density and pre-oxidation of the metal substrate (Banus et al. 2014; Pauletto et al. 2020). The lower the pore density, the more uniform the coating distribution, but the lower the loading of active phase, the poor adhesion and its surface is prone to larger agglomerates and cracks (Santos et al. 2020).

However, the major drawback of the impregnation method is that a macroscopic redistribution of the active phase precursor may occur during drying or calcination of the monolith due to capillary suction (Li et al. 2019). It is difficult to control the thickness and homogeneity of the coating as its lengthy procedures and numerous control parameters (Yang et al. 2006). These factors lead to poor coating quality and a high risk of agglomeration or flaking of the active phase, which is unfavorable for increasing the activity of the catalyst (Banus et al. 2014). What's more, the binder or the acid used in slurry may destroy the structure of the ready-made layer phases (Fu et al. 2022). Ma et al. (2021) pointed out that the original urchin-like Pt-Al_2O_3 and flower-like Pt-ZnO were not maintained after the honeycomb cordierite coating.

Hydrothermal synthesis

The crystallisation of metal salt solutions in high temperature and high pressure environment can generate

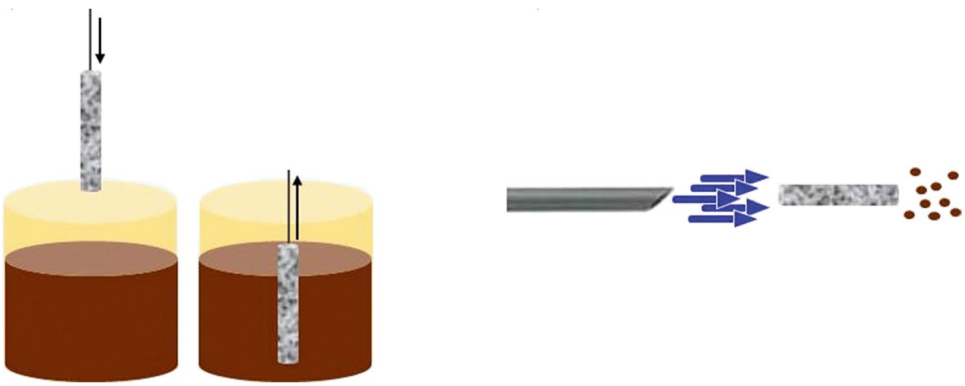

Fig. 8 Impregnation with Pregnation (left) and blowing procedure (right) (Montebelli et al. 2014)

nanocrystals with high crystallinity, uniform particle size and good dispersion. Its application in the preparation of monolithic catalysts is to place supports in a precursor solution to grow the coating or active phase directly on the support through a hydrothermal reaction, as shown in Fig. 9.

Hydrothermal methods are considered to be a typical example of in-situ synthesis of catalytic layers on structural supports. Compared to the dip-coating, this in-situ synthesis provides better access to the support, achieving higher loading and preventing agglomeration and exfoliation of the active phase to a certain extent. Our group developed various metal foam-based monolithic catalysts and found that, compared to other techniques (e.g. impregnation, deposition–precipitation and citric acid complexation), hydrothermal method achieves the highest loading on nickel foam (NF) at the same precursor concentration, which reduces raw material costs (Fig. 10a) (Ni et al. 2022). Based on the redox reaction between $KMnO_4$ and the metal matrix, Chen et al (2019) hydrothermally loaded sodium manganese-type MnO_2 on AISI304 WM and obtained good mechanical stability. The ultrasonic shedding rate of the catalytic layer (160 W/40 kHz/1 h) was only $0.08 \pm 0.03\%$.

Catalysts prepared by hydrothermal methods can be regulated by various means. Our research group adopted a secondary hydrothermal method whereby the Ni-based LDO and MnO_2 layer were hydrothermally loaded successively on NF (Chen et al. 2022a). During the synthesis process, the redox reaction between $MnO_4^-$and Ni^{2+} leads to a LDO intermediates on Mn/NF, which endows the catalysts a higher specific surface area, Mn^3/Mn^{4+}, Ni^{3+}/Ni^{2+} and O_{ads}/

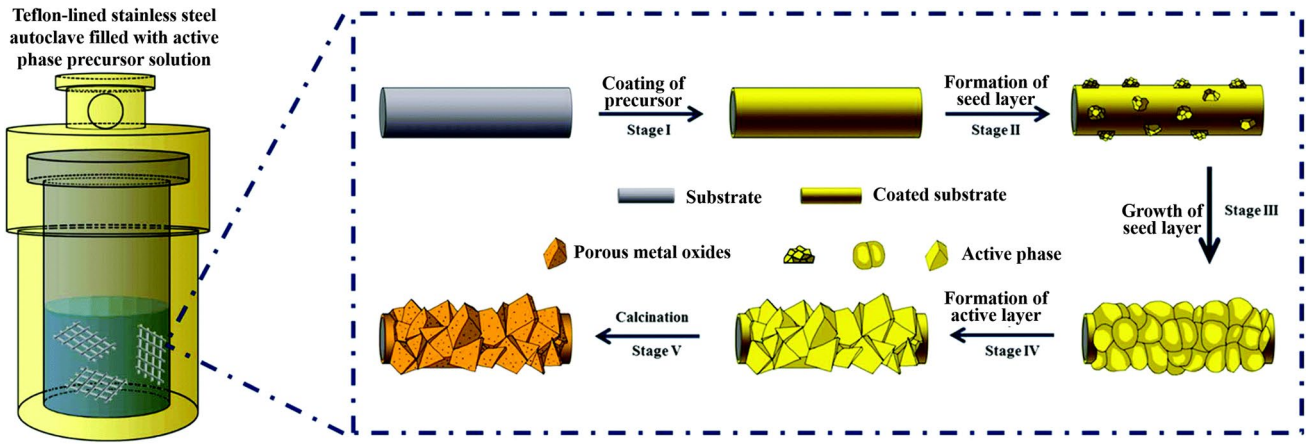

Fig. 9 Growth of the active phase on the substrate in the hydrothermal method (Cai et al. 2017)

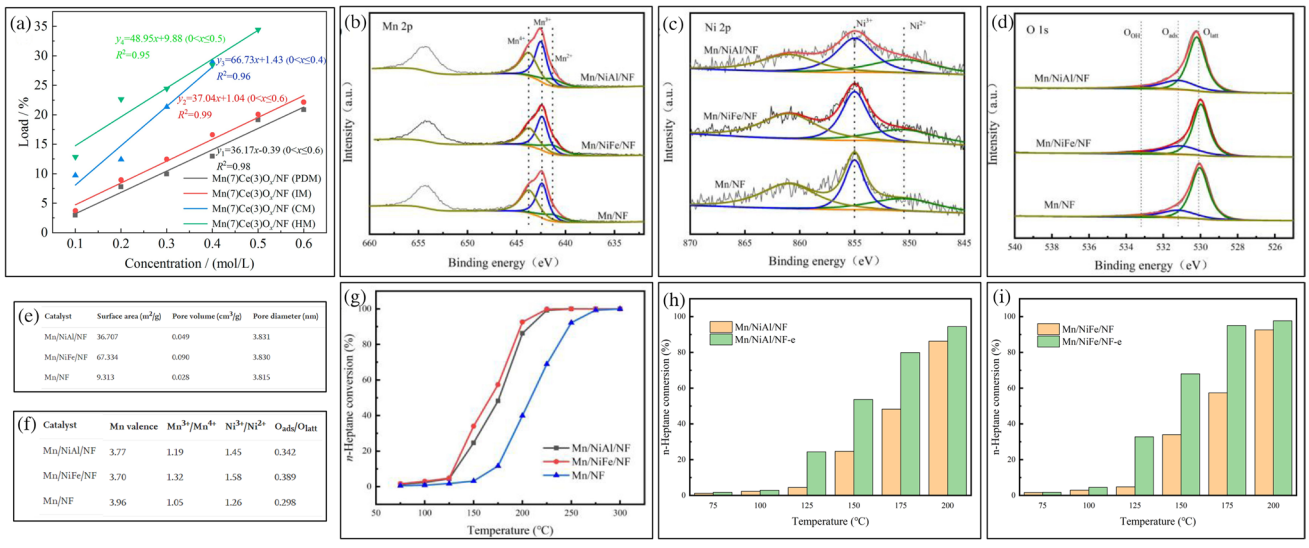

Fig. 10 Loading changes with precursor concentration (**a**) (Ni et al. 2022); XPS profiles (**b–d**), specific surface area and mesoporous parameters (**e**), surface chemical compositions (**f**) and catalytic activity for the samples (**g-h**) (e: electrothermal catalysis) (Chen et al. 2022a)

O_{latt}, thus resulting in a promoted activity, in Fig. 10(b–g). Finally, the catalysts were test in the electrothermal and thermal catalysis. It is speculated that the superior activity under direct current Fig. 10(h–i) is closely related to the electronic effects. For the electrocatalytic reduction of formaldehyde to methanol, a post thermal treatment was proposed to enhance the stability of bimetallic loaded Cu foam electrodes. Despite the desired phenomenon were not happened, high levels of electrochemical activity were obtained which might be attributed to the simultaneous oxidation of Cu substrate and loaded metals. Yin et al (2019) adopted a modified hydrothermal method to grow ZIF-67 membrane on paper-like stainless steel fibers (PSSF), in which a surface modification and seed-induced growth method are proposed (Fig. 11). That is, PSSF is first subjected to a hydrothermal reaction in a 3-aminopropyltriethoxysilane (APTES) / ethanol solution for surface modification. Then the modified PSSF support is aging in a organic linker (2-methylimidazole, Hmim) /metal precursors mixed solutions for generating a seed layer. Finally, a growth process under solvothermal condition was implemented to produce ZIF-67 membrane on the seeded PSSF support. After these three steps, a uniform and dense ZIF-67 membrane is grabbed on the PSSF. Here in, the $-NH_2$ groups on APTES-modified PSSF acted as a covalent linker to combine with the free Zn^{2+} centers of the ZIF-8 precursor, increasing the nucleation sites of heterogeneous nanoscale crystals and the formation of membranes.

However, extensive research has also exposed the shortcomings of hydrothermal method in terms of uneven loading and poor adhesion, which should be highlighted in subsequent studies.

Electrochemical

In electrodeposition, pre-deposited colloidal particles or metal ions are attracted to a opposite charged electrode (usually a coating substrate) under a DC electric field, thus coating the catalytic layer (Vorob'eva et al. 2000; Yang et al. 2003), Fig. 12a. The common electrodeposition methods are Electrophoretic Deposition (EPD) and Electrochemical Deposition (ECD). Both methods are based on the same principles, but their application varies from the electrolyte solution used.

Electrophoretic deposition, which mostly works on particles or colloidal suspensions, was originally developed to obtain alumina pre-coating and is the preferred technology next to impregnation (Yang et al. 2003). Vorob'eva et al. (2000) used alumina sols (hydrolyzed from aluminium isopropoxide) as a suspension during EPD. After drying and calcination, a regular alumina layer with a high specific surface area (450 m^2/g) was obtained on stainless steel mesh. Yang et al. (2003) prepared suspensions from aluminium powder, after which polyacrylic acid and aluminium isopropoxide were added to improve the adhesion of the aluminium powder and regulate the electrical conductivity of the suspensions, respectively. Finally, an Al layer approximately 100–120 μm thick was deposited on the stainless steel wire mesh, followed by calcination to form a porous Al_2O_3 layer. At present, EPD has also been applied for the deposition of other coatings, e.g. graphene oxide (Yuan et al. 2022), TiO_2 (Gómez et al. 2021; Yang et al, 2006), and etc. In addition to the intermediate pre-coatings, a kind of metal composite coatings is also achieved. Zhang et al. (2022b) obtained Ce-doped $NiMn_2O_4$ spinel coatings on ferritic stainless steels by electrophoretic deposition followed by oxidation treatment. The dense Ce-doped $NiMn_2O_4$ spinel coating improves the oxidation resistance of SS, blocking the diffusion of Cr and O atoms during thermal treatment.

Electrochemical deposition, also known as Electroless plating (ELP). By reducing positively charged metal ions at the cathode, a metal coating is formed on the substrate. ECD method is an alternative to realizing metal active phase deposition. Cetina-Dorantes et al. (2021) prepared Co-Mn spinels on stainless steel with metal nitrate solution as electrolyte. Gómez et al. (2019) electrodeposited NiMo/Ni 3D spherical nanocatalyst on 316L SS. The surface of the catalyst was rough and porous, as shown in Fig. 12b. Shen et al.

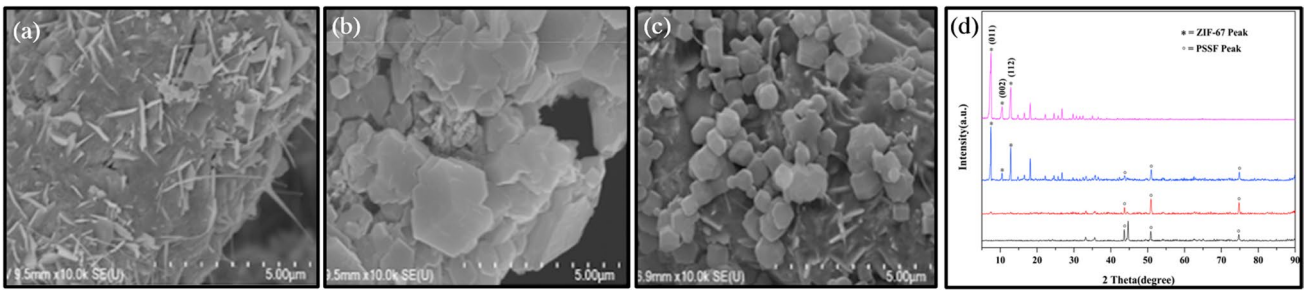

Fig. 11 SEM images of the PSSF (**a**), ZIF-67/PSSF without (**b**) or with (**c**) APTES pretreatment, and XRD patterns (**d**) of the samples: N and W for without and with APTES modification (Yin et al. 2019)

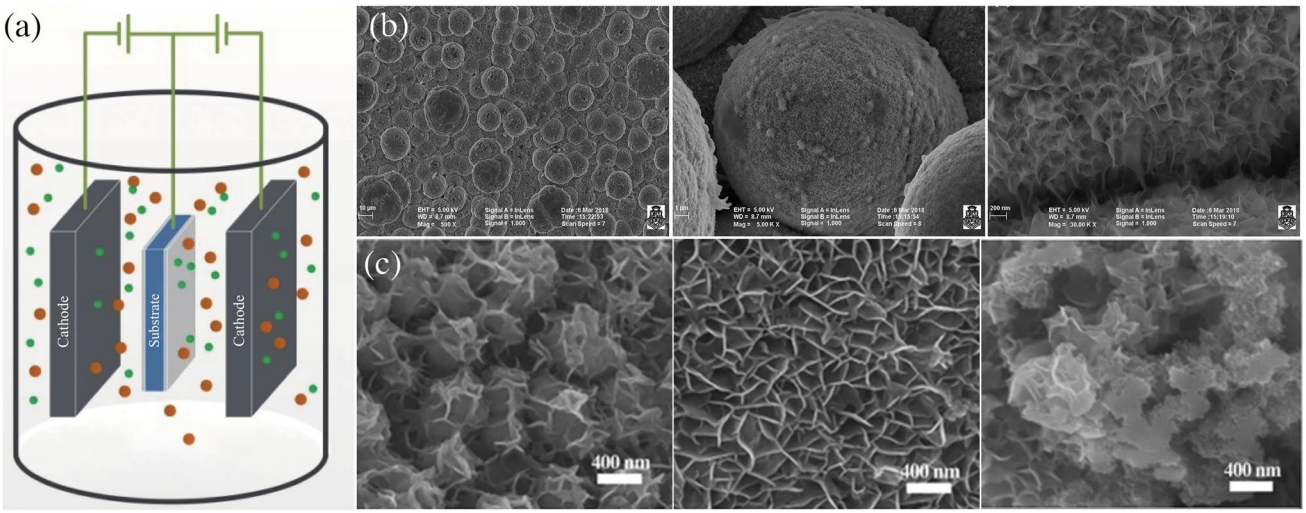

Fig. 12 Scheme of Electrochemical method (**a**) (Sun et al. 2021); SEM image of NiMo-electrodeposited catalyst measured at different magnifications (**b**) (Gómez et al., 2019), and Effect of electrodeposition time on surface morphology of NiFe-LDH/SSF (**c**): 30 s (left), 120 s (middle), and 600 s (right) (Zhu et al. 2020)

(2018) electrodeposited nickel hydroxide or nickel oxide on AISI 304 plate pretreated by electrochemical corrosion (acid or alkali). Ling et al. (2013) designed and reported a preparation method of ZSM-5-Cu/SS catalyst. That is, the stainless steel was first pretreated by anodic oxidation. Then Cu was deposited by ECD, and finally, the ZSM-5 molecular sieve film was covered on the Cu/SS by hydrothermal synthesis.

In electrochemical methods, the thickness and morphology of the coating depend mainly on the chemistry of the electrolyte (such as pH, type and content of additives), electrode spacing, voltage and deposition time, etc. Wunsch et al. (2002) studied the influence of different media (glycerol, oxalic acid, alumina gel) on the coating. The results show that Al_2O_3 colloidal suspension in oxalic acid is not adhesive enough, whereas the addition of alumina gel or glycerol resulted in an adherent layer of 2–4 µm. Serrano et al. (2018) found that the positive or negative surface charge density of TiO_2 could be modulated by adding different stabilizers. This implies that it can select an anodic or cathodic deposition according to the application. Zhu et al. (2020) found that the effect of the electrodeposition time on NiFe-LDH/SS electrode is mainly reflected in the change of morphology. As shown in Fig. 12c, for samples with a deposition time < 120 s, a uniform sheet structure cannot be formed in a short time. Conversely, on samples with deposition times > 120 s, the pretty compact three-dimensional porous structures begins to agglomerate, covering most of the open interlaced nanopores and reducing the contact area between the solution and the active sites, which is not conducive to gas precipitation. In addition, an excess of hydroxide layer will reduce the conductivity of the electrode. The superior catalytic performance of SSF@NiFe is finally related to the hydroxide species and the SSF substrate. That is, the NiFe hydroxide improves the wettability and electrolyte permeability of the electrodes, the average oxidation state of Ni and metallic Ni improve the catalytic activity and conductivity of the nanosheets, respectively, Fe changes the local environment of the nickel hydroxide, resulting in a more stable structure.

Within the variety of coating methods, the electrodeposition has several advantages, such as shorter deposition time, mild conditions, simple and cheap equipment, little restriction of the shape of substrates, which is allow for deposition on both inside and outside surface of the cavities, applicability to powders with a wide range of particle sizes (from micro- to nanometric).

Deposition–precipitation

With the help of precipitates (usually an alkali solution, e.g. ammonia solution or urea), the metal salts in the solution will precipitate on the metal substrate to form a uniform active phase layer. Koo et al. (2016) prepared Ni/$MgAl_2O_4$/FeCrAl by wash-coating and deposition–precipitation (DP), and the results showed that wash-coating gave a thick coating layer (21 µm), which block the channels as well as cause a cracked surface. On the contrary, the monolith catalyst prepared by DP method exhibited a much thicker (1.1 µm) and homogeneous coating without blockage, thus achieving more active sites and long-term stability (Fig. 13).

There are various preparation parameters for the DP method such as aging temperature and time, types of precursors and precipitant, and solution pH. Koo et al. (2017)

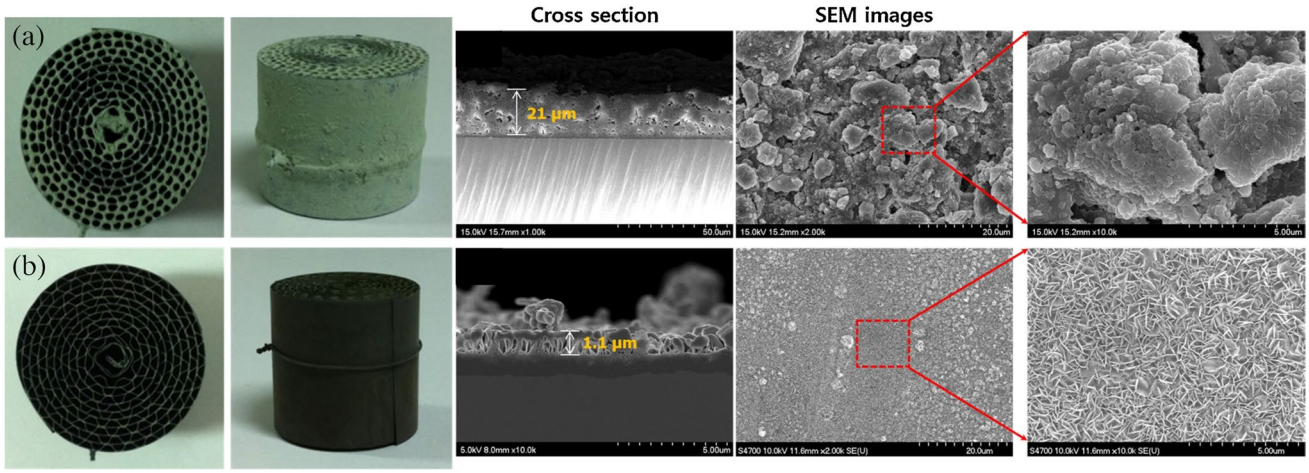

Fig. 13 Photos and SEM images of monolith catalysts coated by (**a**) wash-coating and (**b**) DP method (Koo et al, 2016)

studies the effect of pH and found that it is closely associated with the dispersion, size, and shape of the metal phase. ICP–MS was confirmed that catalysts prepared at pH 10 showed the lowest loading of Ru (0.045 wt.%). This is because the precipitation process is not completed within the precursor solution. SEM images showed that the smallest Ru particles were highly dispersed on the surface of monolith prepared at pH 7. Conversely, the agglomeration of large Ru particles was observed in case of pH 6 and pH 8, as shown in Fig. 14.

Although many metal monolithic catalysts with good activity have been synthesized by DP, the coating adheres weakly too. In addition, to ensure accurate deposition of the active phase on the support, two points must be noted: 1) to ensure a homogeneous solution and to avoid precipitation of metal salts in the body solution; 2) The nucleation rate on the surface of the support must be higher than that in solution.

Chemical vapor deposition

Conventional catalyst preparation methods often require drying, calcination and reduction steps, which lead to sintering of the structure and thus reduce the active surface area. Chemical Vapor Deposition (CVD) is a simple and effective method, which eliminates all of these steps by in-situ growth of catalytic coating in an atmosphere full of active phase precursors. Qi et al. (2017) used the CVD method to deposit a stable K layer on calcined FeCrAl wire mesh. The results showed that the good adhesion of the K layer can be attributed to the formation of K–O-Al species. Researchers (Zhou et al. 2017, 2020) found that the CuO microcrystals

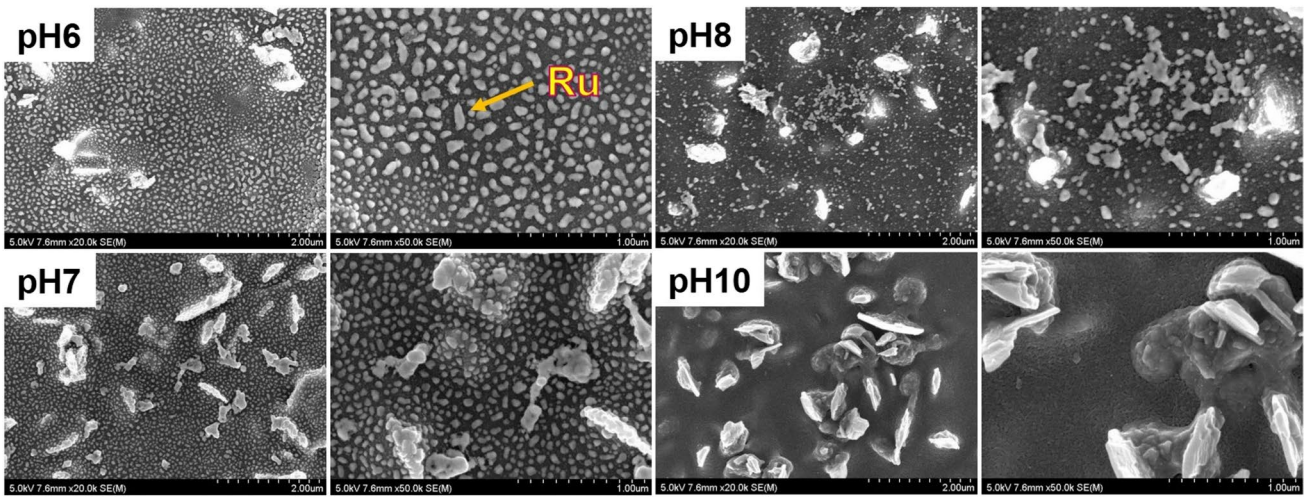

Fig. 14 SEM images of Ru-coated FeCrAlloy catalysts prepared by DP method with different solution pHs (Koo et al., 2017)

prepared by CVD were smaller in size and more evenly distributed than those prepared by impregnation. In addition, the dendrite growth effect also caused an increase in the specific surface area of the support, which promoted the catalytic oxidation of acetone. Kouotou et al. (2016) used Pulsed Spray Chemical Vapor Deposition (PSE-CVD) to deposit a homogeneous layer of Co_3O_4 film on the stainless steel grid.

Atomic Layer Deposition (ALD) is an improved form of CVD. Unlike the hybrid mode of CVD, this process alternates the catalyst precursor with an inert gas feed, resulting in a more homogeneous film.

Ion implantation

Ion implantation is a kind of low-temperature method; its principle is to introduce metal ions with an energy of 20–40 keV in an electrically conductive support (Fig. 8a) (Honcharov et al. 2016). It solves the problem of loading difficulties with conventional deposition methods on nonporous supports (glass, metal, ceramic) (Sanzhak et al. 2018).

Ion implantation procedure does not introduce any crystalline phases of metals or its compounds, but a metallic amorphous state, which indicated by the absence of a reflex of implanted metal and its compounds in SAXS (Fig. 15b) (Honcharov et al. 2016) and XRD (Fig. 15c) (Sanzhak et al. 2018). XPS shows that the amorphous layer is existed as oxides, nitrides, and oxynitrides, while thermal treatment leads to oxidation of oxynitrides to oxides, and nitrides to the oxynitrides, respectively (Sanzhak et al. 2018).

Other advantages of ion implantation include absence of a mechanical and temperature deformation of the sample (the heating of the sample < 100 ℃) (Nikolaieva et al. 2021); a significant change in the surface roughness (Fig. 15d) to further deposit an impregnated coating; superior joule-heating performance (Fig. 15e) to be applied in the electrothermal catalysis (Honcharov et al. 2016) and clean conditions for the process. However, to date, this method has not been practically used in catalyst preparation. Therefore, the studies of the application of ionic implantation in supported metal-based catalyst synthesis are very emergency.

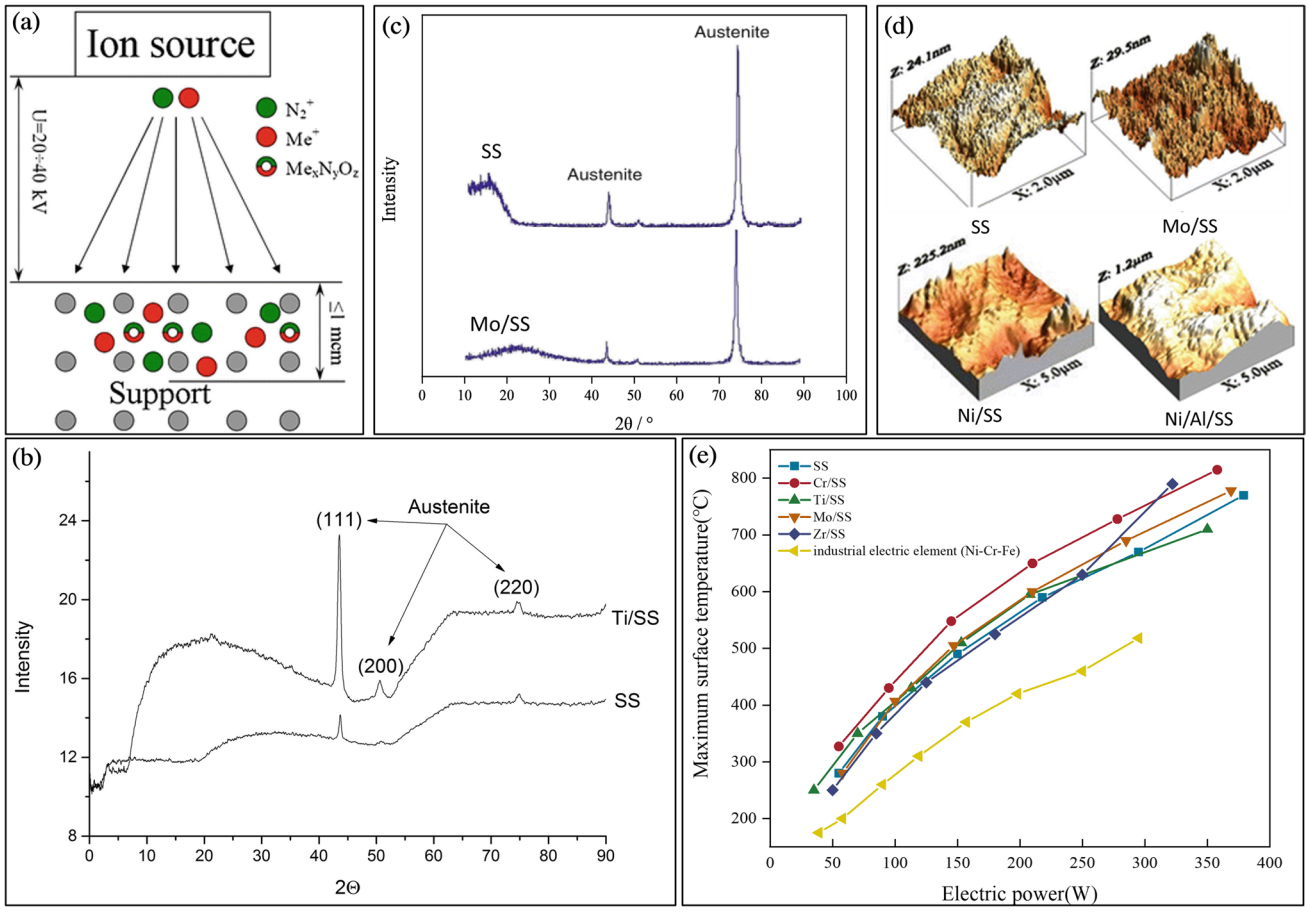

Fig. 15 Scheme of ion implantation (**a**); XRD (**b**), SAXS (C), AFM (**d**) and Joule-heating performance (**e**) of the implanted samples (Honcharov et al. 2016; Sanzhak et al. 2018)

Spraying

Spraying deposits a solution containing active phase precursors on the substrate. When the catalyst is deactivated during subsequent applications, it does not need to be replaced but only repainted, thus offering the advantage of simplicity and low maintenance costs.

Compared with other methods, the spraying method has significant advantages. For example, Wu et al. (2001) compared plasma spraying and dip-coating methods using FeCrAl metal mesh as the substrate and Al_2O_3 as the target coating. It was revealed that the adhesion of coating obtained by the spraying method was stronger with the same coating thickness. Ahlström-Silversand and Odenbrand (1997) coated a porous alumina powder layer on the stainless steel mesh substrate by plasma spraying. A catalyst (Pd/Pt or V_2O_5/CuO) coating was then prepared by impregnation, proving that the spraying could be easily combined with impregnation. In order to reduce the cost of plasma spraying, Li et al. (2018) prepared a stable Pt nanoparticle suspension (shelf life up to 30 d), after which well-dispersed Pt nanocatalysts were obtained on the surface of FeCrAl fibres by simple spraying (Fig. 16). The pore size and porosity of the sprayed coatings depends strongly on the particle size and the deposition rate. In a study of Garcia-Lobato et al. (2019), TiO_2 coatings were sprayed on 316L SS. It was found that a small particle size in sol solution and lower deposition rate promote the formation of a flat and more compact coating. Whereas, a rough and porous structure obtained on a high deposition rate.

Etching

In consideration of the large number of alloying elements in SS, Etching/Corrosion of SS to achieve surface activation is a simple and effective preparation scheme. In etching, the substrate is placed in an alkaline or oxidant solution without the addition of a pre-deposited metal salt, Fig. 17. After a period of hydrothermal treatment (Huang et al. 2021), a catalytic layer can be obtained on the stainless steel.

However, different from other methods, the catalytic layer obtained by etching has a single composition, mostly iron or nickel hydroxides, but the morphology and

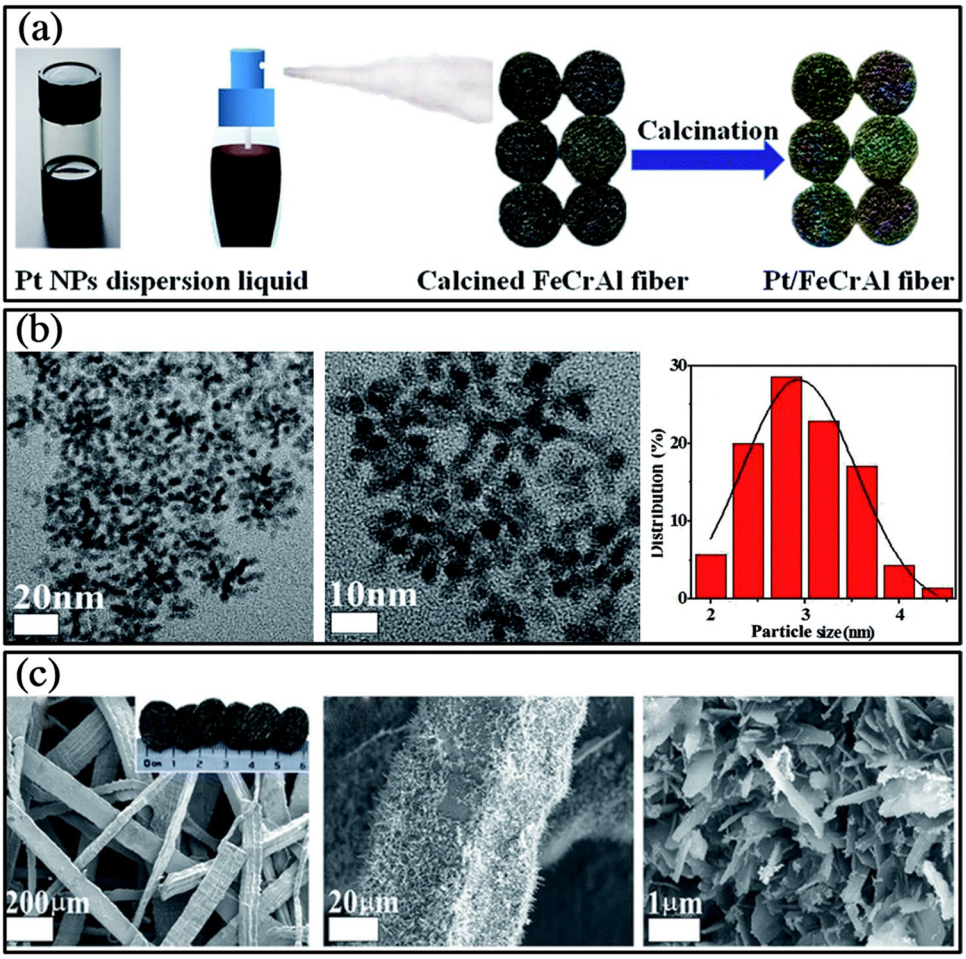

Fig. 16 Suspension spraying for preparing Pt/FeCrAl fiber catalyst (**a**); TEM images of Pt NPs in dispersion liquid and corresponding size histograms(**b**), and SEM images 0.1Pt/FeCrAl fiber (**c**) (Li et al. 2018)

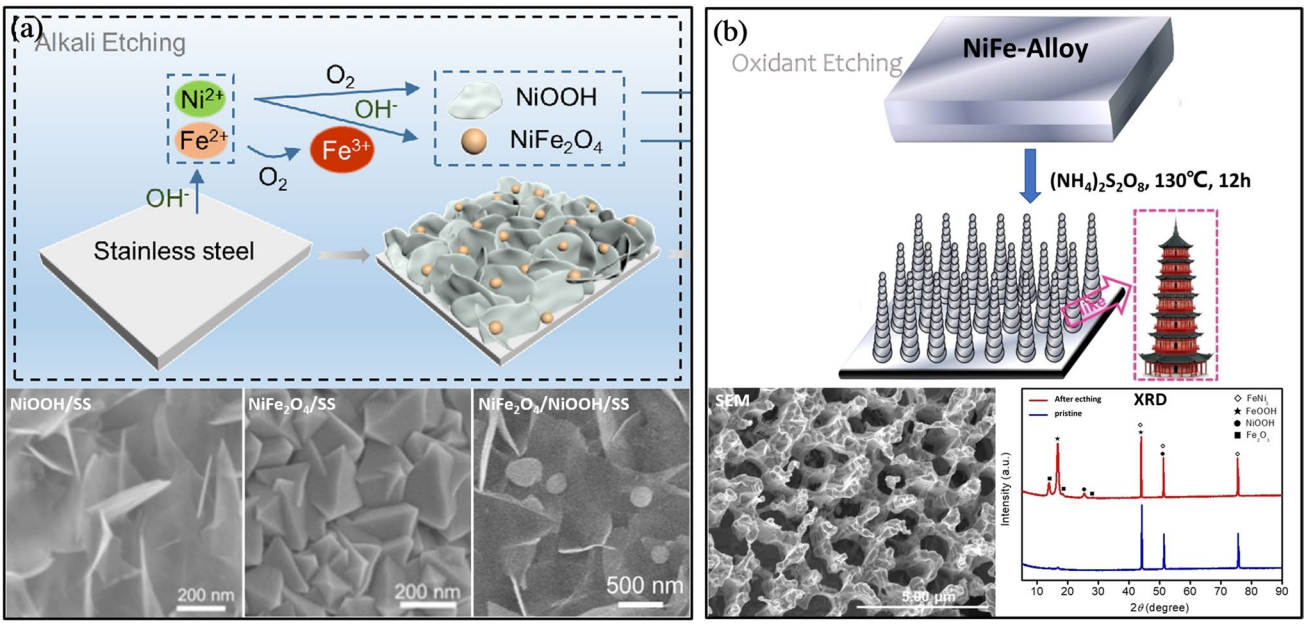

Fig. 17 The preparation process, SEM and XRD of alkali etched $NiFe_2O_4$/NiOOH/SS (Huang et al. 2021) (**a**) and oxidant etched NiFe-Alloy (Chen et al., 2022c) (**b**)

composition of the products can be regulated by modulating the types and concentrations of agents or etching time. Huang et al. (2021) used KOH solution for the hydrothermal etching of SS. The results show that Fe^{2+} and Ni^{2+} are firstly precipitated and then oxidized into Fe^{3+} and Ni^{3+}. At first, due to the low concentration of Ni^{3+}, NiOOH nucleates and gradually grows to nanosheets. Later, as the reaction time increases and the concentration of Fe^{3+} approaches the critical concentration, Fe^{3+} starts to react with Ni^{2+} to form $NiFe_2O_4$ nanoparticles, forming NiOOH/$NiFe_2O_4$ heterostructures. Therefore, by adjusting the reaction temperature, time and OH^- concentration, the leaching rates of Fe and Ni ions can be easily controlled, resulting in different catalytic layers. In their study, pure NiOOH nanosheets were obtained at 6 M and 150 ℃, pure $NiFe_2O_4$ nanocrystals were obtained at 12 M and 200 ℃, while good 3D $NiFe_2O_4$/NiOOH heterostructures were obtained at 6 M and 160 ℃, see Fig. 17b. Chen et al. (2022c) choose $(NH_4)_2S_2O_8$ as a strong oxidant to form a Ni–Fe oxyhydroxide pagoda-shaped nanocone on SS, which mainly exists as Fe_2O_3, FeOOH and NiOOH.

Others

Other preparation methods were also studied. Wu et al. (2005) developed a powder-embedded aluminization technique to improve the adhesion of Al_2O_3 coatings on FeCrAl. Porsin et al. (2016) developed a solution crystallization method to obtain alumina coating with good adhesion on stainless steel wire mesh, which can be carried out at lower temperatures and concentrations. Marbán et al. reported for the first time an ammonia evaporation-induced method for preparing stainless steel wire meshes loaded with $Co(OH)_2/Co_3O_4$. Further doping of K (2014, 2012) and Cu (2010) through impregnation can then be used for catalytic reactions.

Hypothesis and limitations of the develop method

Although many methods have been developed for the preparation of metal-based catalysts, the appropriate technology should be selected according to the actual situation. Figure 18 provides advice on the choice of coating techniques. Spraying and EPD are mostly suitable for flat or corrugated surfaces; whereas dip-coating and CVD are more widely applicable and can provide a homogeneous coating even for complex 3D structures such as honeycombs or foams. In contrast, the wash-coating cannot be applied to wire meshes with wire diameters less than 50 µm (Vorob'eva et al. 2000).

Several points should also be noted during preparation: The interaction between the pretreatment and the active phase coating method should be carefully examined. Li et al. (2017a) electrodeposited Pd species on anodized and calcined FeCrAl-alloy, respectively. Despite the smaller particle size and better dispersion of Pd particles obtained on FeCrAl-anode, Pd/FeCrAl-cal exhibited better catalytic, Fig. 19(a–c). They attribute this paradoxical phenomenon to the different growth mechanisms of palladium on these substrates. On flat surface of FeCrAl-anodic, palladium

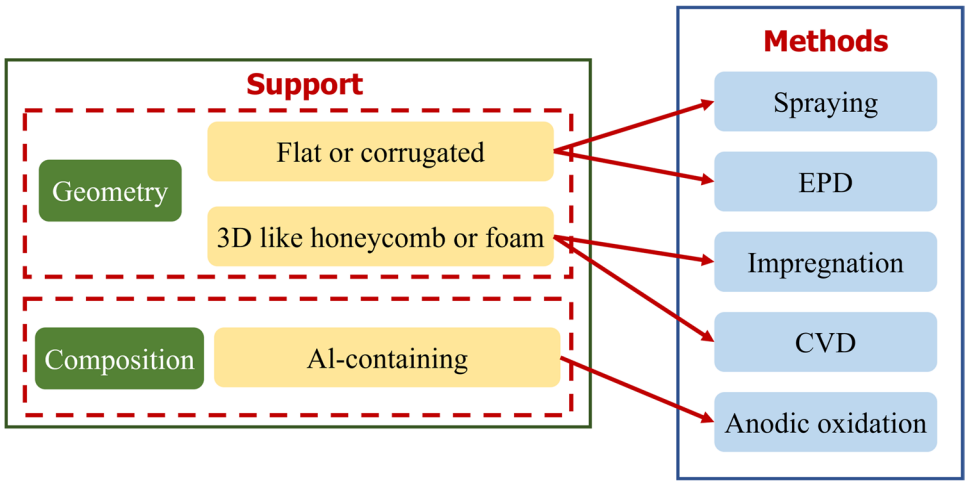

Fig. 18 Advice on methods chosen based on scenarios

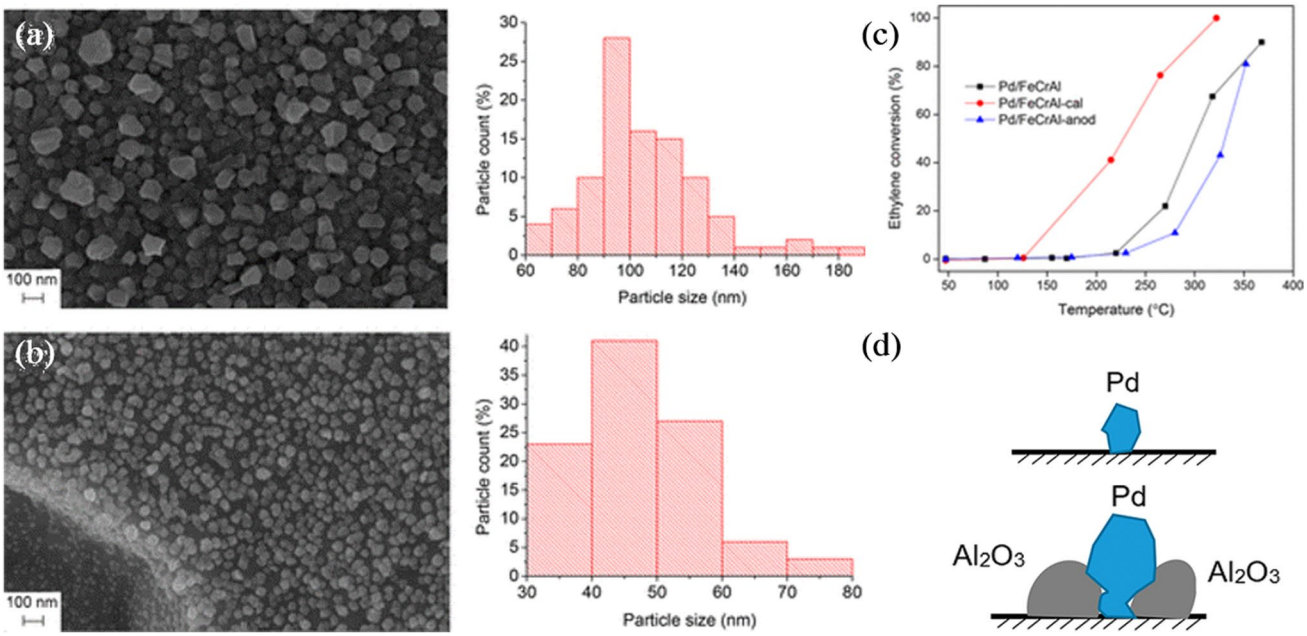

Fig. 19 SEM images and particle size distributions of Pd/FeCrAl-cal (**a**) and Pd/FeCrAl-anod (**b**); Electrothermal catalysis of ethylene on FeCrAl-based Pd catalysts (**c**); Illustration of electroplated palladium particles on FeCrAl-anod (top) and FeCrAl-cal (bottom) (Li et al, 2017a)

particles is lay on the substrate (Fig. 19d), whereas on oxide covered surfaces of FeCrAl-cal, Pd particles preferentially grow from the metal gap between adjacent oxides. The close contact of the metal oxide with the palladium particles can alter the oxidation state of the palladium and favor the formation of partial palladium oxide; The strong Pd-metal oxide interactions produce sufficient oxygen species and give a better explanation towards the higher catalytic activity of Pd/FeCrAl-cal. Moreover, although it is recognized that metal oxide precoating benefits higher specific loading (loading of active phase per unit geometric surface area) of ceramic supports, the need for a pre-coating for metal substrates should be determined on a case-by-case basis. Barbero et al. 2008 further coated MnCu catalysts on FeCrAl alloys precoated with an alumina layer and found that the alumina layer reduced the loading of the active phase and catalytic activity. Not coincidentally, a similar phenomenon was observed by Santos et al. (Santos et al. 2020). The reason for this may be that the alumina coating covers the whiskers formed by high temperature calcination, thus reducing the surface roughness and decreasing the amount of active components attached.

Application of stainless steel catalyst in gaseous pollutant control

Diesel exhaust soot control

With its high torque, high efficiency and long life, diesel engines play a vital role in the socio-economic development and transportation industry (Hoang 2021). However, the carcinogenic exhaust gases they produce deeply troubled the diesel industry. Amongst these soot particles are a complex mixture of carbon black, metal ash, hydrocarbons, water and sulfur compounds. Due to their small size, they can penetrate deep into the human lungs and pose a cancer risk (Geng et al. 2022). As a result, increasingly stringent legislation has been established to regulate soot emissions.

Despite significant advances in engine design, fuel pretreatment, combustion process modification, fuel injection strategies and fuel formulation, post-processing equipment is still indispensable (Peng et al. 2023; Yu et al. 2021a). Catalytic Diesel Particulate Filter (CDPF) has the greatest potential among all treatment methods. The filter can collect soot particles and performs soot combustion on the wall coated with a catalytic layer (Mei et al. 2021; Lin et al. 2018). Stainless steel has been extensively investigated as its thermal expansivity is similar to that of engine components, allowing the catalyst to be installed closer to the engine and facilitating rapid ignition of the automotive catalyst to meet more stringent emission control regulations.

A variety of active components effective for soot combustion have been applied to the development of stainless steel CDPF, such as Ce, Mn. Chen et al. (2019) obtained MnO_2/SS catalyst through redox reaction between $KMnO_4$ and AISI 304 and explored the influence of calcination temperature, Fig. 20a. It was found that α-MnO_2 was the dominant active phase on samples calcined at temperatures below 600 °C, while $MnCrO_3$ promoted the adhesion of the active phase as an intermediate layer. However, when temperature continued to increase to 700 °C, $MnCrO_3$ became the dominant active phase. Meanwhile, higher valence Mn species are generated and more Cr^{6+} and Fe^{3+} doped in the active layer, which favoured the activation of O_2 to O_2^{2-} or O_2^- and the generation of oxygen vacancies. Moreover, MSS700 with the largest amount of K^+ dopants and surface oxygen enables quickly chemisorption of O_2, thus accelerating surface oxygen mobility and forming oxygen vacancies. The soot oxidation mechanism of MnO_2/SS at different roasting temperatures is shown in Fig. 20(b–c). For MSS550, the substitution of Mn ions by Cr and Fe dopants enhances the transfer of lattice oxygen to its surface and the formation of reactive oxygen species (O*). Finally, the gaseous O_2 replenishes the depleted active oxygen following the following pathway. $O_2 \rightarrow O_{ads}$ (adsorbed oxygen) $\rightarrow O_s$ (surface oxygen) $\rightarrow O_{latt}$ (lattice oxygen). On the (201) face of $MnCrO_3$ of MSS700, the abundant surface oxygen species can oxidise soot, resulting in the formation of surface oxygen vacancies. More Cr^{6+} and Fe^{3+} dopants would then generate a large number of oxygen vacancies that could be occupied by gaseous O_2 via the following pathway: $O_2 \rightarrow O_{ads} \rightarrow O_s$. Bruneel et al. (2012) deposited Cu/Mo/Ce catalytic layer on sintered FeCrAl-alloy short fibre multi-layer filter constructed by

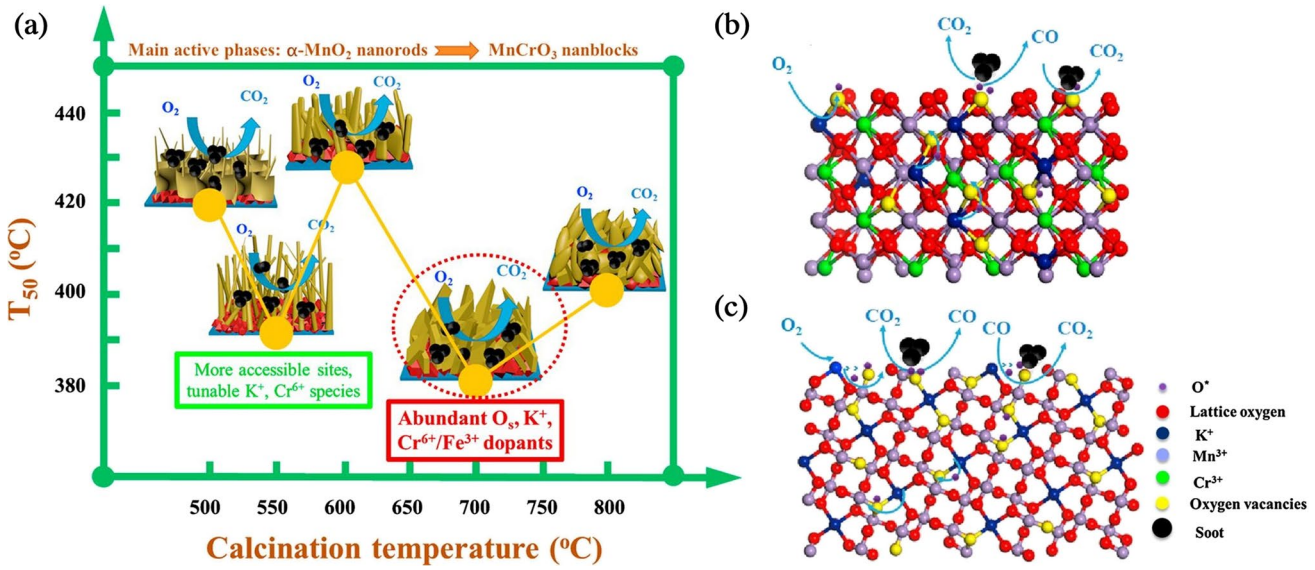

Fig. 20 Effect of calcination temperature on MnO_2/SS (**a**), and mechanism illustration of soot combustion over MSS700 (201) facet (**b**), MSS550 (310) facet (**c**) (Chen et al. 2019)

Bekaert N.V. Company, which reduced the soot burning temperature by at least 75 ℃, while avoiding the corrosion of substrate and ensuring good adhesion.

Alkali metal elements can promote soot combustion by wetting soot particles, regulating soot electron distribution or activating oxygen (Chen et al. 2019). In particular, K-containing catalysts have soot combustion activity comparable to that of precious metal catalysts. Considering that K corrodes ceramic supports and reduces their mechanical properties, especially in the case of thermal shock (Qi et al. 2017), mechanically stable stainless steel carriers are an important breakthrough for obtaining thermally stable and high-efficiency catalysts. Banús et al. prepared Co-Ba-K/ZrO_2/SS catalysts with good mechanical and thermal stability by wash-coating method, which are based on AISI 304 wire mesh (2014) and AISI 314 foam (2010), respectively. The results showed that both catalysts exhibited excellent soot oxidation activity. The activation energy of the AISI 314 foam catalyst was 92 kJ/mol, which was equivalent to that of Co-Ba-K/ZrO_2 powder catalyst (82 kJ/mol). Qi et al. (2017) deposited K in-situ on the commercial FeCrAl wire meshes by CVD. The deposited K interacted strongly with the calcined Al_2O_3 layer, forming a stable K–O-Al species. The performance of the catalyst was comparable to that of commercial CDPF, with soot ignition occurring at 350 ℃ and remaining stable for 5 cycles. However, K-containing catalysts are susceptible to pyrolysis during the reaction, especially for K_2CO_3 and KNO_3 (Wang et al. 2018). A effective approach to balance the stability and activity in K-based catalyst is incorporating K^+ in silicate glass (Zokoe et al. 2019). Su and McGinn (2014) developed a glass catalyst based on SS substrate(K_2O-CaO-SiO_2/SS). As shown in Fig. 21, as the reaction progressed, sublimated K^+-containing vapor accumulates on the glass surface through ion exchange, resulting in the formation of KOH and K_2CO_3, which reduces the soot oxidation temperature and provides long-term stability of the oxidation cycle.

Considering the complex exhaust composition of diesel engines (Singh et al. 2022), the requirements for purifiers have been extended to the simultaneous removal of multi-component pollutants. Ce based catalysts have proven to be effective for soot purification due to their excellent oxygen storage capacity, and precious metals are a good choice for low-temperature degradation of VOCs. Godoy et al. (2018) prepared a Pt/CeO_2 catalyst on AISI 304 metal mesh cylinders. The results showed that the catalyst exhibited good catalytic activity for the simultaneous removal of VOCs (toluene, n-hexane, ethyl acetate) and soot, where the removal of VOCs occurred at 200–350 ℃, and the combustion of soot occurred at 300–500 ℃. The Co-Ba-K/ZrO_2/AISI 314 foam catalyst prepared by Banús et al. (2010) could achieve simultaneous removal of soot and NOx.

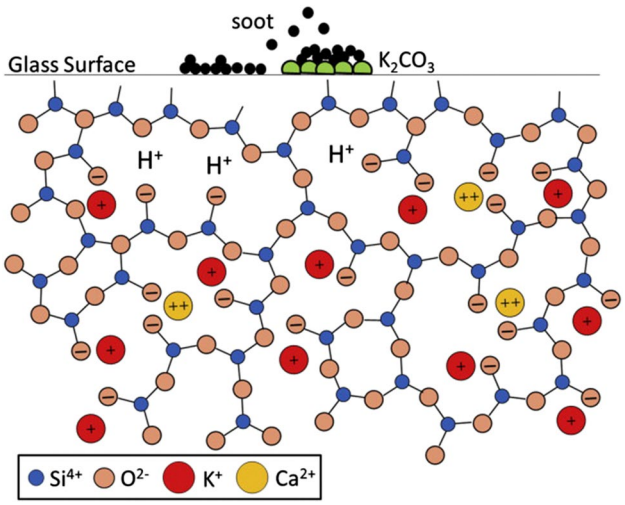

Fig. 21 Schematic diagram of the surface of a catalytic K–Ca–Si–O glass (Su and McGinn 2014)

However, despite great efforts to reduce the temperature of soot oxidation, such as optimizing the catalyst composition and improving the catalyst-soot contact efficiency, the ignition temperature of soot (T_{10}, temperature at which the conversion efficiency reaches 10%), remains > 200 ℃ (Mei et al. 2021).

VOCs emission control

Worldwide, the accelerated pace of urbanization and industrialization has led to a dramatic increase in emissions of volatile organic compounds (VOCs) (Mo et al. 2020). In addition to their inherent toxicity, teratogenicity and carcinogenicity, VOCs are also the main culprits for the formation of secondary pollutants, such as tropospheric ozone, peroxyacetyl nitrate and secondary organic aerosols (He et al. 2019). Given the environmental impact and toxicity of VOCs and the increasingly stringent regulations, it is important to design effective methods to reduce VOCs emissions.

Catalytic combustion is a convenient, energy-saving and effective method (Zhao et al. 2019). By selecting the right catalyst, it can catalyze the deep decomposition of VOCs into CO_2 and H_2O at lower temperatures (200 – 500 ℃). Stainless steel is inexpensive and widely available, and its rich elemental composition makes it a potential catalyst support for VOC oxidation.

A major application limitation of metal-based monolithic catalysts is the difficulty in obtaining high loading amounts of active components. Therefore, noble metals are a good choice to ensure satisfactory activities, as shown in Table 4. Yang et al. obtained Ti/TiO_2 (2006) and Al/Al_2O_3 (2004a, 2004b) porous coatings on WMH by EPD, and then achieved Pt/TiO_2/Ti or Pt-TiO_2/Al/Al_2O_3 coated WMH catalysts by

Table 4 Application of noble metal-based SS catalyst in VOCs emission control

Catalyst	Contaminant	Concentration/(ppm)	Atmosphere	GHSV/(h^{-1})	T_{98}/(℃)	Ref
1.0%Pt/Ti/ TiO_2/SS	Ethyl acetate	1000	Air	2000	280*	Yang et al. (2006)
0.1% Pd-0.05%Pt/SS	Toluene	1000–1600	Air	10 000	180	Zhang et al. (2012)
	Acetone	1700–2500			240	
1.0%Pt-TiO_2/Al/Al_2O_3/WMH	Ethyl acetate	1000	Air	2000	290	Yang et al. (2004a)
1.0%Pt-TiO_2/Al/Al_2O_3/ WMH	Methanol	1000	Air	2000	130	Yang et al. (2004b)
	Benzene				180	
	Toluene				190	
	Ethanol				260	
	n-hexane				280	
	Ethyl acetate				310	
0.1%Pt-0.02%Pd/SS	Acetone	1700–2500	Air	10 000	160	Zhang et al. (2010)
0.1%Pt-0.5%Pd /SS	Toluene	1000–1600	Air	10,000	220	Ma et al. (2008)
	Acetone	1700–2500			260	
	Ethyl acetate	1100–1700			280	
0.01% Pt -0.02%Pd/SS	Toluene	700 ~ 900	Air	6000	210	Li et al. (2003)
0.01% Pt -0.02%Pd/SS	Toluene	1000–1600	Air	10,000	210	Chen et al. (2008)
0.1%Pd-6%Mn/SS	Toluene	1000–1600	Air	10,000	260	Song et al. (2009)
	Acetone	1700–2500			220	
	Ethyl acetate	1100–1700			320	
0.75%Ce-0.1%Pt-0.5%Pd/SS	Toluene	1000–1600	Air	10,000	160	Chen et al. (2009)
	Acetone	1700–2500			220	
	Ethyl acetate	1100–1700			250	

*Gaseous hourly space velocity, GHSV.

impregnation respectively. When applied to the catalytic combustion of VOCs, it was found that the WMH catalysts were consistently much more active than the CH catalysts, which is due to the significant external mass transfer rate difference between CH and WMH. Chen Min's group (Chen et al. 2008; Li et al. 2003; Ma et al. 2008; Zhang et al. 2012, 2010) prepared a series of Pt- and Pd- based SSWM catalysts for the removal of VOCs (such as toluene, acetone and ethyl acetate), and achieved satisfactory catalytic activity. Later, in order to further improve the catalytic activity and reduce the loading of noble metals, they doped transition metals in the catalysts, such as Pd-Mn /SSWM (Song et al. 2009) and Ce-Pt–Pd/SSWM (Chen et al. 2009). The activity of the catalysts was found to be related to the excellent oxygen storage and release properties of the transition metals and the strong synergistic effect with Pd.

Althoucgh noble metal-based SS catalysts have achieved promising catalytic activity, transition metals with low prices and wide sources have always been a hot topic within the VOCs purification, as shown in Table 5. Mn and Co with various valence states have been considered as ideal substitutes for noble metal catalysts because of their excellent physicochemical and easy synthesis. The composition and flexible structure of SS is of great significance to the oxidation of VOCs. Duran et al. (2011) loaded MnOx on austenitic SS (AISI 304), which was subsequently used for the combustion catalysis of ethyl acetate. The results showed that Fe- and Mn-rich SS promoted the adhesion of the active components through chemical affinity, and the solid solution reaction between Mn_2O_3 and Fe_2O_3 led to a significant improvement of the catalyst performance compared to the pure oxide. Li et al. (2021) prepared Co_3O_4 on MWH by a one-step hydrothermal reaction and used it for the catalytic oxidation of formaldehyde. Compared with Co_3O_4 powder (T_{100} = 160 ℃), Co_3O_4@SSM exhibited better catalytic activity (T_{100} = 130 ℃) and stability, which was attributed to the higher specific surface area, Co^{3+}/Co^{2+}, O_{latt}/O_{ads}, and the difference in morphology, as shown in Fig. 22. The SSM substrate makes Co_3O_4 grow vertically in the form of porous needle-like nanoribbons, which reduces agglomeration and overlap, promotes the exposure of more adsorption and active sites. Moreover, the fully exposed pore structure is conducive to the diffusion of HCHO on the catalyst surface. Luo et al. (2019) synthesized a new MnOx/PSSF-embedded activated carbon catalyst (Mn-GAC/PSSF) for catalytic oxidation of methyl ethyl ketone (MEK) by a papermaking process and impregnation method. The results showed that the activity of Mn-GAC /PSSF was better than that of Mn-GAC due to the excellent mass transfer and contact efficiency of PSSF, which favored the complete oxidation of MEK. Topka

Table 5 Application of transition metal-based SS catalyst in VOCs emission control

Catalyst	Contaminant	Concentration / (ppm)	Atmosphere	GHSV /(h^{-1})	Flow rate / ($mL \cdot min^{-1}$)	T_{90} /(°C)	Ref
MnOx/SS	Ethyl acetate	1000	Air	3,000	300	380	Duran et al.(2011)
FeCe-WO_3/WM	Propylene + butene	2500 + 2500	10% $O_2 + N_2$	40,000	-	300	Porsin et al. (2016)
MnOx-FeCrAl	Ethyl acetate	1000	-	3000	-	192	Santos et al. (2020)
Co_3O_4@SSM	Formaldehyde	400	Air		100	120	Li et al. (2021)
$V_2O_5/TiO_2/Al_2O_3$/WMH	1,2—dichloroben-zene	500	Air	2000		240	Yang et al.(2003)
10%Cu-LTA/PSSF	Acetone	1500	Air			300	Zhou et al. (2017)
Co_3O_4@SSGM	Propylene	10,000	5% O_2 + Ar	45,000*	15	380	Kouotou et al.(2016)
	n-butene					400	
Mn-GAC/PSSF	MEK	2000	Air	-	200	280	Luo et al. (2019)
Co-Mn@SS	Ethanol	770	Air	20,000*		244	Topka et al. (2022)
Co_3O_4/SSM	Ethanol	760 ± 10	Air	21,000 ± 1000*		250	Dvorakova et al. (2019)
Co_3O_4/PSSF	Isopropanol	1000	Air	15,000		281	Yan et al. (2022)
Cr/ZSM-5/ PSSF	trichloroethylene	125	Air	19,863		495	Zhang et al. (2020)

*Weight hourly space velocity, $ml \cdot g_{cat}^{-1} \cdot h.^{-1}$

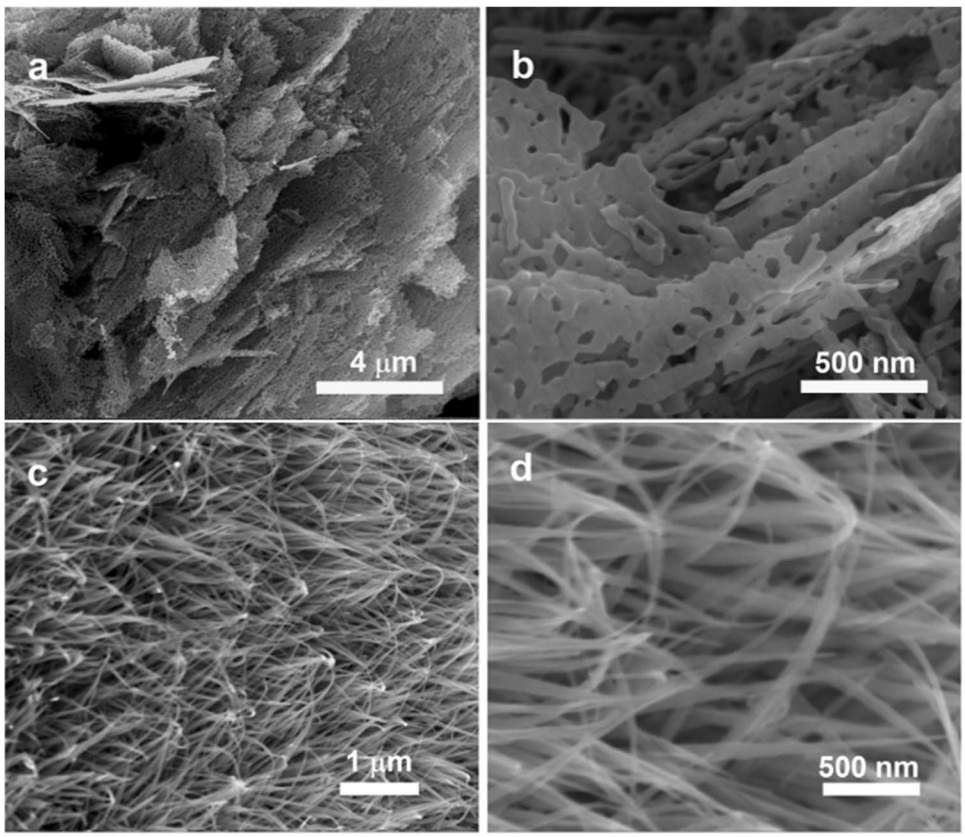

Fig. 22 SEM images of powder (a, b) and CSSM-supported (c, d) Co_3O_4 (Li et al. 2021)

et al. (2022) deposited structured Co-Mn mixed oxides on stainless steel mesh by hydrothermal synthesis. The mesh structure of support made it possible to deposit thin layers of active phase and significantly inhibited the influence of internal diffusion. In the oxidation of ethanol, the activity of this catalyst is 48 ~ 114 times higher than that of a commercial granular Co-Mn-Al catalyst. Yan et al (2022) prepared Co_3O_4 derived from ZIF-67 membranes over PSSF for isopropanol combustion, and compared the effect of calcination temperature on catalytic activity. It is observed that when the

temperature increased from 350 ℃ to 450 ℃, the crystals on the surface of PSSF shrank, the surface area and pore volume reduced significantly. Finally, samples calcined at 400 ℃ with the most uniform particle size and highest content of surface Co^{3+} and O_{ads} show a greater catalytic performance. Zhang et al. (2020) demonstrated that the oxidation of trichloroethylene on Cr/ZSM-5/PSSF composites fits the Mars-van Krevelen kinetic model and relies on the interaction of the oxygen-rich center with the TCE molecules. The activation energy of the surface oxidation was 64.57 kJ/mol and that of surface reduction was 122.25 kJ/mol.

For gas–solid heterogeneous catalytic systems, the key lies in the adsorption of target gas molecules on the active sites and mass migration on the catalyst surface. Inspired by alveoli, Anwer et al. (2021) inoculated ZnO nanorods on stainless steel grids and further loaded flower-like $NiMoO_4$ and modified C_3N_4 to prepare the "cavitation" catalyst, as shown in Fig. 23a. The catalyst was used for catalytic oxidation of toluene and it was found that toluene molecules were preferentially stored in the cavity due to the concentration gradient and the affinity of zinc oxide for toluene molecules. When the adsorption reached saturation, VOC molecules in the cavitation were slowly released and migrated to the $NiMoO_4$ and C_3N_4 active sites, where they are degraded. This alveolar structure overcomes the poor intermolecular interactions at low concentrations and the coverage of catalytic active sites at high concentrations of conventional catalysts. In this way, ZNC@SSM can adapt to different concentration conditions and play stable catalytic oxidation, as shown in Fig. 23b.

DeNOx

NOx emissions from automobile exhaust and stationary sources such as oil/coal-fired power plants, garbage incinerators and chemical plants are the main cause of acid rain, photochemical smog and ozone layer depletion (Chen et al. 2021). Increasingly stringent emission requirements have led to the development of many control technologies.

Selective catalytic reduction (SCR) of ammonia is the dominant technology for denitrification in tail gas (Zhang et al. 2022a). Commercial SCR catalysts are V_2O_5-WO_3/TiO_2 and/or V_2O_5-MoO_3/TiO_2 supported on ceramic honeycomb supports. However, some drawbacks of these catalysts have been identified in practical application. 1) V_2O_5 has a limited temperature window (300 ~ 400 ℃) (Chen et al. 2021; Yu et al. 2021b) and is listed in China's hazardous waste list, its treatment and disposal procedures are cumbersome and costly; 2) Typical NOx-containing exhaust gases are often accompanied by SO_2, H_2O and soot. V_2O_5 also shows high catalytic activity for the conversion of SO_2 to SO_3 (Yao et al. 2006). The ammonium sulfate (Shu et al. 2012a) and metal sulfate species (Shu et al. 2014) formed will be deposited on the surfaces of pipes and heat transfer

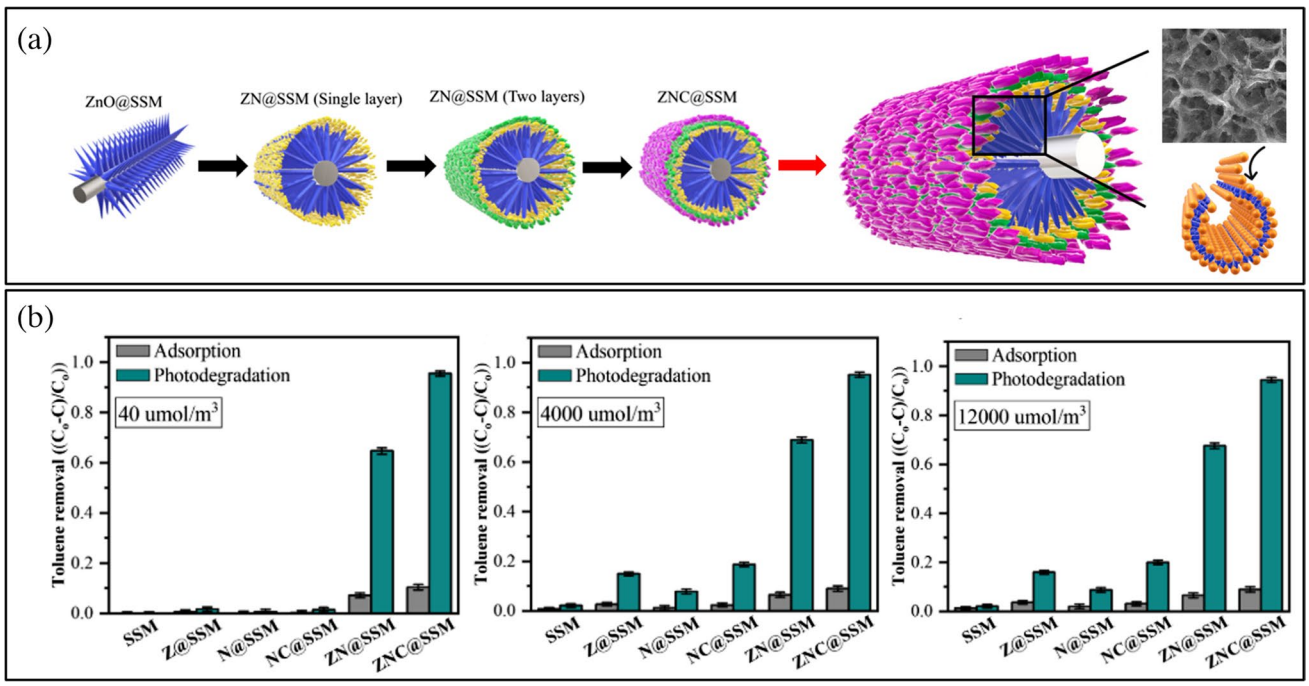

Fig. 23 (**a**) Schematic diagram of "alveoli" catalyst, Inset: SEM image of ZNC@SSM (top) and (bottom) Toluene adsorption on catalyst surface, yellow pellets for VOC, blue for "cavitation" skeleton. (**b**) Toluene removal by photodegradation and adsorption at different input concentrations, in which both ZNC@SSM and ZN@SSM are "alveoli" catalysts (Anwer et al. 2021)

equipment, causing corrosion, blockage and heat loss, and leading to coverage and inactivation of active sites. Dust (Shu et al. 2014) can clog the channel structure of the ceramic honeycomb, leading to a significant decrease in the effective utilization rate of catalyst.

Therefore, it is of great significance to seek alternative metal elements and cs. Fe_2O_3 has been shown to be effective for SCR reaction. Shu et al. (2012b) prepared Fe modified Ce/TiO_2 catalyst and found that the addition of Fe significantly improved the low-temperature SCR activity, N_2 selectivity and resistance to sulphur poisoning of the catalysts, Fig. 24a. Therefore, Fe-rich stainless steel is a promising SCR catalyst or support. Table 6 is a summary of stainless steel based catalysts used in SCR applications.

Porsin et al. (2016) prepared FeCeW catalysts supported on SSWM and obtained excellent SCR catalytic activity. Shu et al. compared the SCR reactivity of V_2O_5-WO_3/TiO_2 on different supports (WMH and CH), Fig. 24b. It was found that the activity of the WMH catalyst was significantly higher than that of CH catalyst at a lower temperature (≤ 125 ℃), which might be due to the promotion effect of stainless steel substrate (Cr25Al5) on the conversion of NOx. While

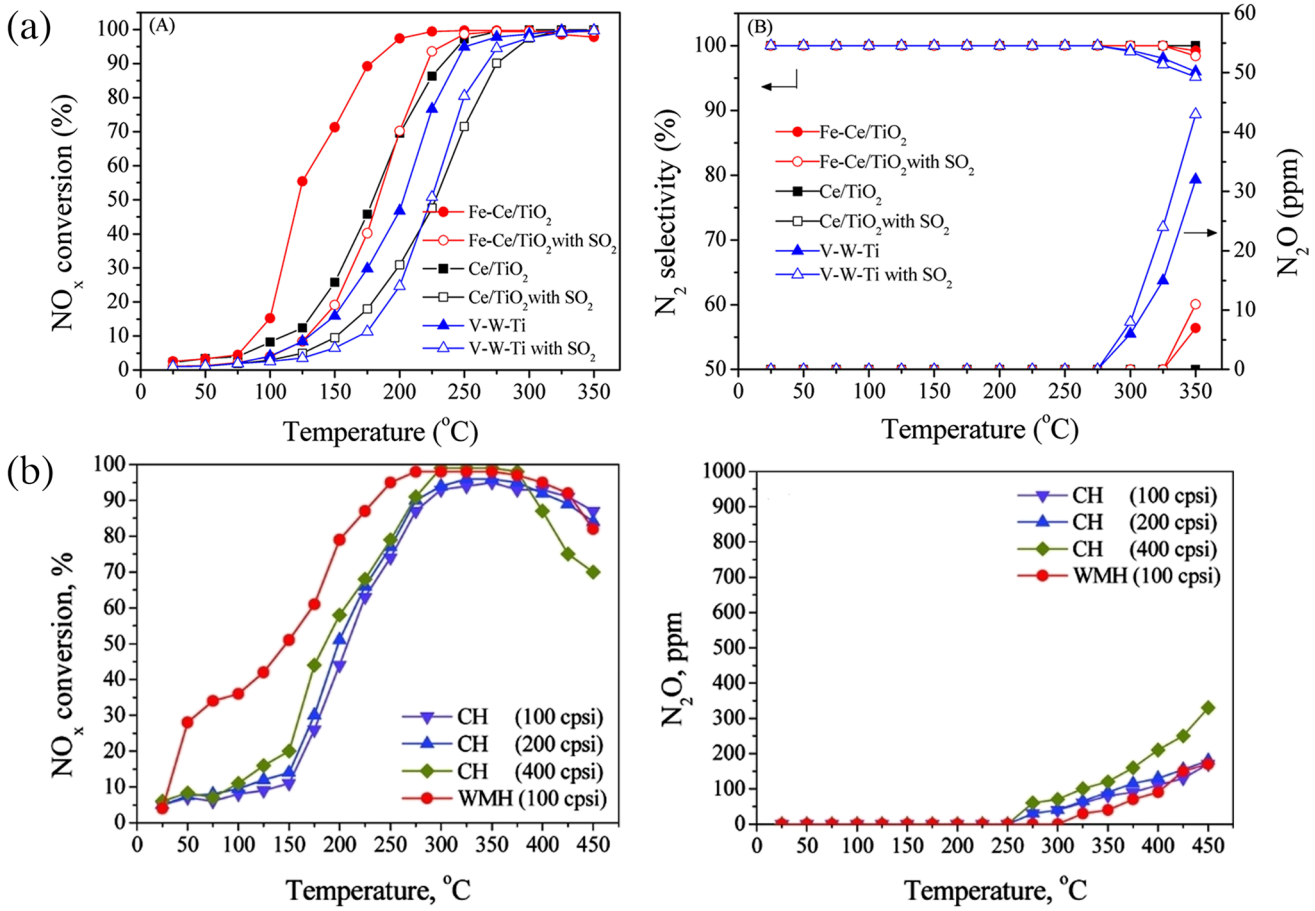

Fig. 24 (**a**) The influence of Fe on the catalytic activity、N_2 selectivity and sulfur-poisoning resistance of the catalyst. (Shu et al. 2012b) (**b**) The SCR activity of WMH and CH catalysts (Shu et al. 2012a)

Table 6 Stainless steel SCR catalyst

Catalyst	NO /(ppm)	NH_3 /(ppm)	Atmosphere	GHSV /(h^{-1})	T_{95} /(℃)	Ref
V_2O_5-$WO_3/TiO_2/Al_2O_3$/WMH	1000	1000	3% O_2+N_2	10,000	225	Shu et al. (2012a)
V_2O_5-$WO_3/TiO_2/Al_2O_3$/WMH	500	500	21%O_2+N_2	5000	250	Yao et al. (2006)
FeCe-WO_3/WM	750	800	0.005%NO_2+10%O_2+N_2	40,000	400	Porsin et al. (2016)
Ce-Fe/TiO_2/Al_2O_3/WMH	1000	1000	3% O_2+N_2	30,000	175	Shu et al. (2012b)
Ce-Fe/TiO_2/Al_2O_3/WMH	1000	1000	0.1%SO_2+3%O_2+N_2	10,000	250	Shu et al. (2014)
V_2O_5-$WO_3/TiO_2/Al_2O_3$/WMH	900	1000	3% O_2+N_2	2000	200	Sun et al. (2010)

in the temperature range of 150 ~ 225 ℃, the difference in activity between WMH and CH catalyst increased with the increase of temperature. This is because the amplified effect of mass transfer rate on catalytic activity at higher temperatures. In addition, WMH catalysts have a wider temperature window (250–425 ℃) and less N_2O yield.

Under lean combustion conditions, a large amount of incompletely burned hydrocarbons are still present in engine exhausts. Hydrocarbon selective catalytic reduction (HC-SCR), which directly uses these hydrocarbons as reducing agents, is expected to achieve the simultaneous removal of VOCs and NOx from motor vehicle exhaust and is a promising emission control method (Gholami et al. 2020). Sun et al. (2008b) investigated the ability of $Pd/Ce_{0.66}Zr_{0.34}O_2/TiO_2/Al_2O_3$/SSWMH catalysts for the selective catalytic reduction of NOx from propylene under lean combustion conditions and compared it with pellet and CH catalysts. The honeycomb catalyst was found to exhibit the best low-temperature catalytic activity, with NOx conversion up to 74.0% at 140 °C, and it can stabilize rapidly in a short time after the temperature increased.

N_2O degradation

N_2O is an important ozone-depleting agent and greenhouse gas. Its global warming potential is 300 times higher than that of CO_2. The main anthropogenic sources of N_2O are adipic acid and nitric acid industries, combustion of fossil fuels and biomass, fertilizer plants and denitrification processes (SCR and three-way catalytic converter). N_2O is highly stable in the atmosphere and can exist in a free state for 120 years. As a result, its degradation requires high temperature and energy (Akça et al. 2021). Great efforts have been made to reduce anthropogenic N_2O emissions, among which catalytic decomposition technology does not require any reducing reactants to achieve the conversion of N_2O to N_2 in the presence of a catalyst (Kim et al. 2019; Klegova et al. 2019).

In light of the advantages of high gas turbulence and high thermal conductivity, stainless steel wire monolithic support has been widely used in N_2O decomposition. Klyushina et al. (2015) and del Rio and Marban (2012) prepared K-Co_3O_4/SS catalyst by electrodeposition and ammonia evaporation-induced method respectively and performed N_2O catalytic decomposition tests in the laboratory. According to H_2-TPR, they concluded that the redox cycle between Co^{2+} and Co^{3+} is a key step for N_2O degradation, and it is the interaction between K and Co_3O_4, making the number of active sites and temperature required for the unwanted reduction of Co^{2+} to metallic Co much higher. The comparision among the K/Co_3O_4 supported on SS or TiO_2 pellets and granular ones have shown that these novel SS-structured catalysts have the highest specific activity, kinetic constant, which is due to its highest H_2 consumptions per mol of cobalt and lowest internal diffusion resistance. In other words, SS substrate make full use of the active components disposed in the catalyst. Ho et al. (2020) synthesized a Rh/Mg/Al hydrotalcite-derived film on the surface of FeCrAl foam and compared its N_2O degradation performance with the pelletized counterpart, Fig. 25. It was found that both catalysts exhibited comparable de-N_2O performance, but lower activation energy was obtained for the structured catalyst.

Selective oxidation of NH_3 (SCO)

In the ammonia industry, increasing attention has been paid to the treatment of ammonia in waste gas. Selective catalytic oxidation (SCO) of ammonia is a promising technology for

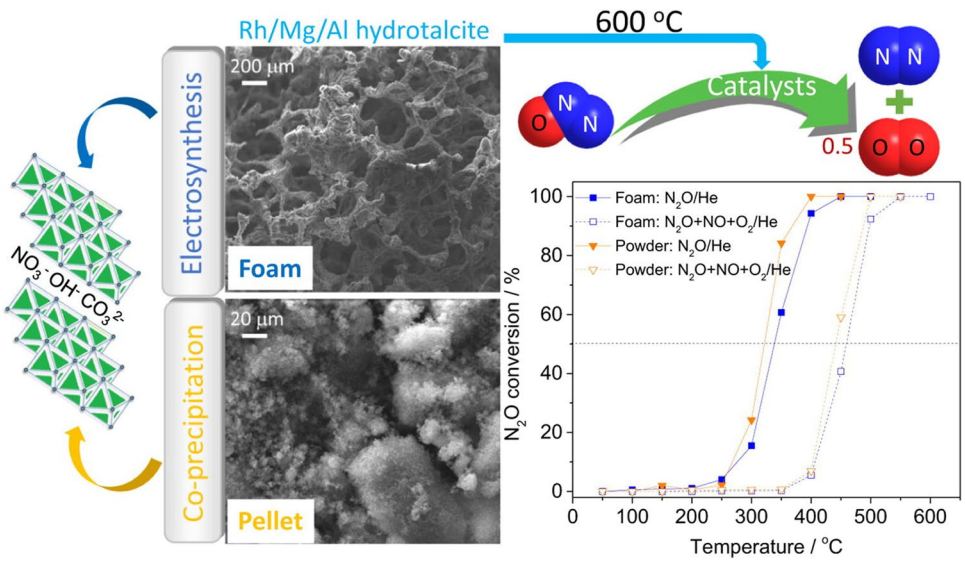

Fig. 25 Schematic diagram of catalytic decomposition of N_2O by Rh/Mg/Al-FeCrAl foam (Ho et al. 2020)

the conversion of NH_3 to harmless N_2 and H_2O (Wang et al. 2022a, 2022b). Qu et al. (2013) prepared a series of metal wire honeycomb catalysts loaded with Ag and Cu, and found that the presence of Ag obtained a higher NH_3 conversion rate, while Cu is conducive to promoting N_2 selectivity.

Future applications

Sterilization

At the end of 2019, the outbreak of COVID-19 caused a huge shock to human society and economic development. Airborne droplets are reported to be the main transmission route for respiratory diseases (Wang et al. 2021). Therefore, air bacteriostasis is an important guarantee for human safety and health in the current environment.

Membrane filtration enables the interception of solid pollutants in the air and has the advantages of high efficiency, energy-saving and ease of large-scale application. It is a mainstream air purification technology. To obtain a filter film with appropriate pore size, Zhong and Xiong. (2021) prepared a composite coating film on stainless steel mesh by combining spraying with gas-induced phase separation technique. The porous membrane was composed of the polystyrene-butadiene block copolymer and TiO_2 nanoparticles, which has good permeability and reduced air pressure (< 100 Pa). The filtration efficiency of *E. coli* in the air is as high as 99.7%. Meanwhile, TiO_2 nanoparticles in the coating film showed a photocatalytic sterilization efficiency of 99.6%, proving the application prospect of this system in air purification, as shown in Fig. 26.

Electrothermal catalysis

In order to overcome the disadvantages of large size, high energy consumption, and slow preheating of catalytic system in the traditional heating mode, a self-heating mode of the catalyst was developed based on the Joule-heating effect of electrothermal elements (Pauletto et al. 2020). It converts the input electrical energy into heat energy by using the resistance loss inside the material, so as to achieve effective heating of the catalytic bed. This electrothermal catalytic mode combines the heater and catalyst bed into one, allowing flexible control of system temperature by adjusting the input electrical power, resulting in reduced equipment size, improved energy efficiency, and rapid reaction ignition.

As a conductor, stainless steel has appropriate resistance to suit this pattern well, which made it widely used in the degradation of gas pollutants and methane reforming reaction. Li et al. prepared FeCrAl electrothermal catalysts loaded with Pd (2017a) and MnOx (2017b) for the catalytic oxidation of CO, toluene and ethylene, respectively. As shown in Fig. 27. It is obvious that electrothermal catalysis gives higher catalytic activity. Rieks et al. (2015) prepared $LaNi_{0.95}Ru_{0.05}O_3$/FeCrAl catalyst for dry reforming of methane. Labrecque and Lavoie (2011) used steel wool as catalyst support and electric heating element to conduct methane dry reforming. The current was found to have a strong effect on the conversion of both methane and carbon dioxide. Zhou et al. (Guo et al. 2011a, 2011b; Zhou et al. 2008) developed a novel plate electrothermal catalyst using commercial sheet aluminium cladding alloy Al/Fe–Cr-Ni alloy/Al. Zhu et al. (2019b) reported a new FeCrAl electrothermal monolithic catalyst loaded with Pt and Pd, which verified the rapid thermal response capability and stability of the electrothermal mode. This will hopefully enable the storage of renewable energy (solar, wind) and reduce frequent start-up costs of intermittent reactions.

Conclusions

The potential and competitiveness of stainless steel as catalyst or support in gaseous pollution control reflect in the following aspects:

1) Good plasticity is conducive to the flexible manufacturing of reactors and nesting of emission reduction modules. 2) The low clogging network structure and pressure drop adapt to high-velocity and dust-laden applications, it will improve the effective utilization rate of the reactor. 3) The radial mixing of airflow improves the mass and heat transfer rate, and together with the high thermal conductivity

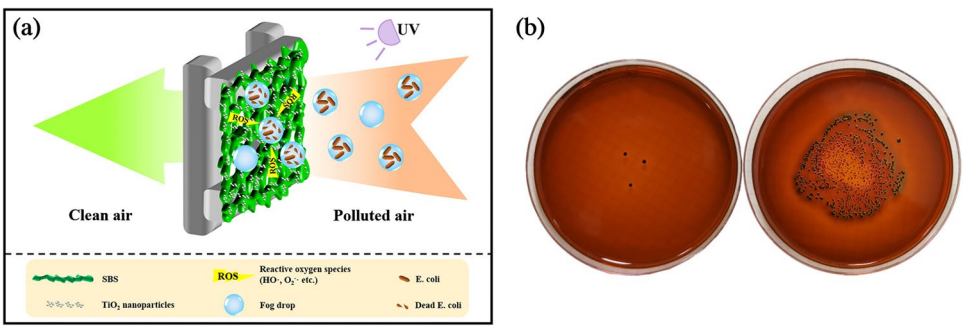

Fig. 26 Schematic of UV-assisted air purification system (**a**), and inactivation effect on the blocked E. coli for the coating films with(left) or without(right) UV light (**b**) (Zhong and Xiong 2021)

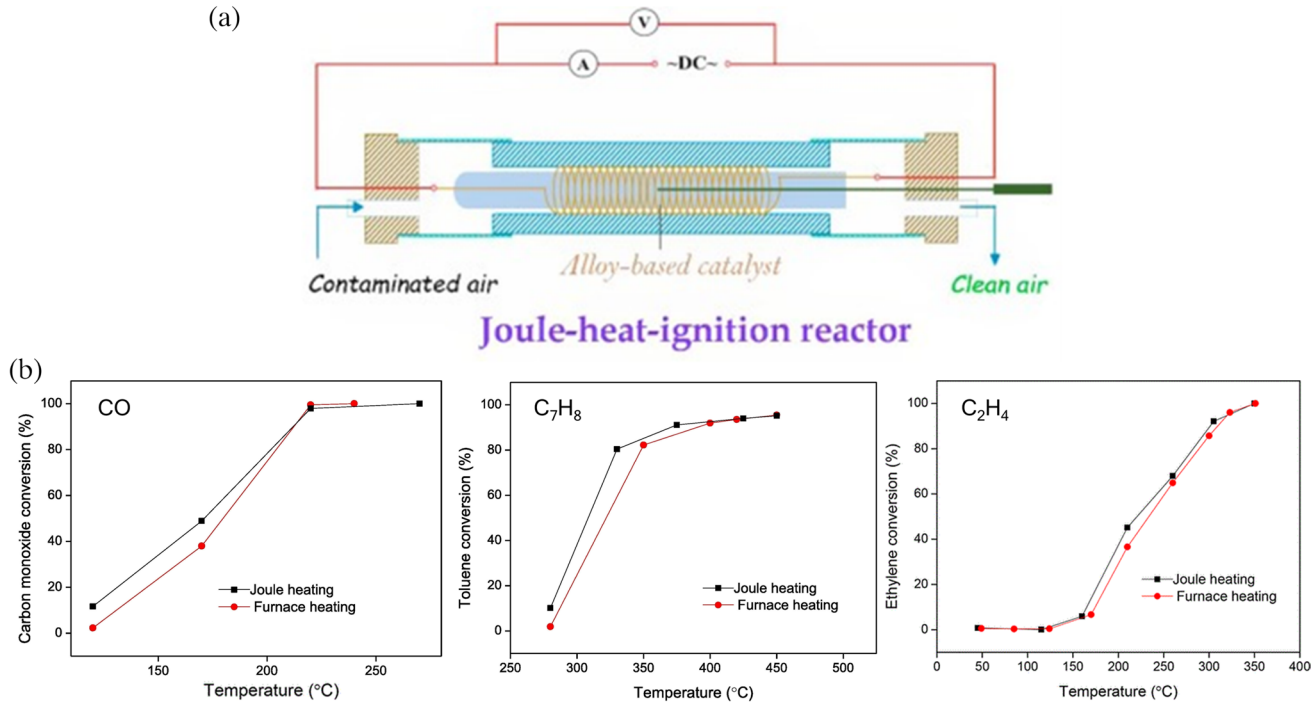

Fig. 27 (**a**) Scheme diagram of joule heating reactor, and (**b**) comparison of thermal and electrothermal catalytic activities of the alloy-based catalysts (Li et al. 2017a, 2017b)

of the skeleton contributes to the uniform distribution of temperature in the catalytic bed, which reduces the generation of local hot spots and avoids the agglomeration and deactivation of active components. 4) The transition metal in it endows a certain catalytic activity, and the possible interaction with the active layer is expected to improve the mechanical property and activity of catalysts. 5) The application prospect of electrothermal catalysis will minimize the reactor volume and catalyst mass, and the rapid thermal response-ability is suitable for intermittent reaction processes (such as catalytic purification of cooking fume and pharmaceutical exhaust gas) and storage of renewable energy (such as wind and solar energy, etc.). It is anticipated that all of the above benefits of SS-based catalysts will not only contribute to the deep or broad management of the atmosphere, but will also facilitate the transition of human society to clean energy, thereby achieving goal of sustainable development.

However, like other metal-based monolithic catalysts, stainless steel based catalysts still have many problems to be solved in the preparation and production. At present, oxide coating on stainless steel substrate is the main method to improve the surface roughness and the adhesion of active layers. Most of the reported catalysts opted for the 'C + I/D' method, that is, coating an oxide layer on stainless steel by wash-coating, electrophoretic deposition, or sol–gel, and followed by loading the active metal by impregnation/dip-coating. This directly leads to a long cycle, cumbersome steps and high cost. Therefore, in this context, the improvement or development of new preparation technology is still a key for the application and popularization of stainless steel or other metal matrices in catalysis. In addition, further exploration of activating/amplifying its potential catalytic activity will also be a major research focus to maximize the application potential of stainless steel in the catalytic industry.

Author contribution All authors contributed to the study conception and design. Shunzheng Zhao and Weixiao Wang put forward the review ideas and organized the first draft. Prof. Honghong Yi, Xiaolong Tang, and Shunzheng Zhao refined and finally approved the whole content. The sections of Electrothermal catalysis were arranged by Chaoqi Chen. All authors commented on previous versions of the manuscript. The final manuscript is read and approved by all authors for publication.

Funding This work was financially supported by National Natural Science Foundation of China (21876010), Fundamental Research Funds for the Central Universities, China (FRF-IDRY-20–018) and Natural Science Foundation of Guangdong Province, China (2020A1515011197).

Data availability The datasets used and/or analyzed during the current study are available in the Web of Science. The copyright permissions of the reproduced figures and tables were achieved.

Declarations

Ethics approval Not applicable.

Consent to participate Not applicable.

Consent for publication Not applicable.

Competing interests The authors declare no competing interests.

References

Agueniou F, Vidal H, Yeste MP, Hernandez-Garrido JC, Cauqui MA, Rodriguez-Izquierdo JM, Calvino JJ, Gatica JM (2020) Ultrathin Washcoat and Very Low Loading Monolithic Catalyst with Outstanding Activity and Stability in Dry Reforming of Methane. Nanomaterials-Basel 10:445–451. https://doi.org/10.3390/nano10030445

Ahlström-Silversand AF, Odenbrand CUI (1997) Thermally sprayed wire-mesh catalysts for the purification of flue gases from small-scale combustion of bio-fuel Catalyst preparation and activity studies. Appl Catal A-Gen 153:177–201. https://doi.org/10.1016/S0926-860X(96)00329-8

Akça A, Karaman O, Karaman C (2021) Mechanistic Insights into Catalytic Reduction of N_2O by CO over Cu-Embedded Graphene: A Density Functional Theory Perspective. ECS J Solid State Sc 10:041003. https://doi.org/10.1149/2162-8777/abf481

Alber KS, Cox JA (1997) Electrochemistry in Solids Prepared by Sol-Gel Processes. Mikrochim Acta 127:131–147. https://doi.org/10.1007/bf01242718

Aljerf LM (2016) Reduction of gas emission resulting from thermal ceramic manufacturing processes through development of industrial conditions. Sci J King Faisal Univ 17:1–10. https://doi.org/10.17632/c4j2c5ks7d.1

Aljerf L (2015) Effect of Thermal-cured Hydraulic Cement Admixtures on the Mechanical Properties of Concrete. InterCeram: Int Ceram Rev 64:346–356. https://doi.org/10.1007/bf03401142

Anantharaj S, Venkatesh M, Salunke AS, Simha T, Prabu V, Kundu S (2017) High-Performance Oxygen Evolution Anode from Stainless Steel via Controlled Surface Oxidation and Cr Removal. Acs Sustain Chem Eng 5:10072–10083. https://doi.org/10.1021/acssuschemeng.7b02090

Anonymous (1982) Appendix IV - Specifications Applicable to Anodic Oxide Coatings on Aluminium. In: Henley VF (Editor), Anodic Oxidation of Aluminium and its Alloys. Pergamon, 163–165. https://doi.org/10.1016/B978-0-08-026726-5.50027-X

Anwer H, Ali M, Lee S, Jeong SH, Park JW (2021) Simulating alveoli-inspired air pockets in a ZnO/$NiMoO_4$/C_3N_4 catalyst filter for toluene entrapment and photodecomposition. J Hazard Mater 409:13https://doi.org/10.1016/j.jhazmat.2020.124497

Baddour CE, Fadlallah F, Nasuhoglu D, Mitra R, Vandsburger L, Meunier JL (2009) A simple thermal CVD method for carbon nanotube synthesis on stainless steel 304 without the addition of an external catalyst. Carbon 47:313–318. https://doi.org/10.1016/j.carbon.2008.10.038

Badmaev SD, Sobyanin VA (2020) Steam reforming of dimethoxymethane to hydrogen-rich gas over bifunctional CuO-ZnO/η-Al_2O_3 catalyst-coated FeCrAl wire mesh. Catal Today 348:9–14. https://doi.org/10.1016/j.cattod.2019.08.050

Banus ED, Milt VG, Miro EE, Ulla MA (2010) Co, Ba, K/ZrO_2 coated onto metallic foam (AISI 314) as a structured catalyst for soot combustion: Coating preparation and characterization. Appl Catal A-Gen 379:95–104. https://doi.org/10.1016/j.apcata.2010.03.009

Banus ED, Sanz O, Milt VG, Miro EE, Montes M (2014) Development of a stacked wire-mesh structure for diesel soot combustion. Chem Eng J 246:353–365. https://doi.org/10.1016/j.cej.2014.02.086

Bao LEI, Wu D (2022) Catalytic properties of $SmMnO_3$/cordierite monolithic catalysts: acid treatment and calcination process optimization using response surface methodology. J Chem Sci 134https://doi.org/10.1007/s12039-022-02042-4

Barbero BP, Costa-Almeida L, Sanz O, Morales MR, Cadus LE, Montes M (2008) Washcoating of metallic monoliths with a MnCu catalyst for catalytic combustion of volatile organic compounds. Chem Eng J 139:430–435. https://doi.org/10.1016/j.cej.2007.12.033

Bello A, Fashedemi OO, Fabiane M, Lekitima JN, Ozoemena KI, Manyala N (2013) Microwave assisted synthesis of MnO_2 on nickel foam-graphene for electrochemical capacitor. Electrochim Acta 114:48–53. https://doi.org/10.1016/j.electacta.2013.09.134

Bortolozzi JP, Banus ED, Milt VG, Gutierrez LB, Ulla MA (2010) The significance of passivation treatments on AISI 314 foam pieces to be used as substrates for catalytic applications. Appl Surf Sci 257:495–502. https://doi.org/10.1016/j.apsusc.2010.07.019

Bruneel E, Van Brabant J, Le MT, Van Driessche I (2012) Deposition of a Cu/Mo/Ce catalyst for diesel soot oxidation on a sintered metal fiber filter with a CeO_2 anti corrosion coating. Catal Commun 25:111–117. https://doi.org/10.1016/j.catcom.2011.12.017

Cai S, Liu J, Zha K, Li H, Shi L, Zhang D (2017) A general strategy for the in situ decoration of porous Mn-Co bi-metal oxides on metal mesh/foam for high performance de-NOx monolith catalysts. Nanoscale 9:5648–5657. https://doi.org/10.1039/c6nr09917c

Carty WM, Lednor PW (1996) Monolithic ceramics and heterogeneous catalysts: Honeycombs and foams. Curr Opin Solid State Mater Sci 1:88–95. https://doi.org/10.1016/S1359-0286(96)80015-5

Cetina-Dorantes M, Lizama-Tzec FI, Estrella-Gutierrez MA, Herrera-Zamora DM, Ares-Muzio O, Oskam G (2021) Electrodeposition of cobalt-manganese oxide selective coatings for solar-thermal applications. Electrochim Acta 391:12. https://doi.org/10.1016/j.electacta.2021.138906

Chang T, Zhang L, Ma RJ, Liu XY (2021) Thin-sheet monolithic-structured Pd-Au-CuOx/M-fiber (M=Ni, Al, SS, Cu) catalysts for gas-phase hydrogenation of dimethyl oxalate to ethylene glycol. Aip Adv 11:5. https://doi.org/10.1063/5.0049310

Chen M, Ma Y, Li GF, Zheng XM (2008) Support effect, thermal stability, and structure feature of toluene combustion catalyst. Catal Commun 9:990–994. https://doi.org/10.1016/j.catcom.2007.09.032

Chen M, Ma Y, Song C, Zhang T, Zheng X (2009) Preparation and Performance of Ce-Pt-Pd/Stainless Steel Wire Meshes Catalyst. Chinese J Catal 30:649–653. https://doi.org/10.1007/s10553-009-0140-8 (in Chinese)

Chen L, Liu G, Feng NJ, Yu JH, Meng J, Fang F, Zhao P, Wang L, Wan H, Guan GF (2019) Effect of calcination temperature on structural properties and catalytic soot combustion activity of MnOx/wire-mesh monoliths. Appl Surf Sci 467–468:1088–1103. https://doi.org/10.1016/j.apsusc.2018.10.223

Chen J, Fu P, Lv D, Chen Y, Fan M, Wu J, Meshram A, Mu B, Li X, Xia Q (2021) Unusual positive effect of SO_2 on Mn-Ce mixed-oxide catalyst for the SCR reaction of NOx with NH_3. Chem Eng J 407:127071. https://doi.org/10.1016/j.cej.2020.127071

Chen C, Zhao S, Tang X, Yi H, Gao F, Yu Q, Liu J, Wang W, Tang T, Meng X (2022a) δ-MnO_2 decorated layered double oxides in-situ grown on nickel foam towards electrothermal catalysis of n-heptane. J Environ Sci-China. https://doi.org/10.1016/j.jes.2022.03.017

Chen L, Zhang D, Chen Y, Liu F, Zhang J, Fu M, Wu J, Ye D (2022b) Porous stainless-steel fibers supported CuCeFeOx/Zeolite catalysts for the enhanced CO oxidation: Experimental and kinetic studies. Chemosphere 291:132778. https://doi.org/10.1016/j.chemosphere.2021.132778

Chen Q, Wang J, Yu K, Xu Z, Sheng X, Shen J, Zhang Q, Liu W (2022c) Green Synthesis of Self-Supported Ni−Fe Oxyhydroxide Pagoda-Shaped Nanocone Arrays for Electrocatalytic Oxygen Evolution Reaction. ChemElectroChem, 9-15https://doi.org/10.1002/celc.202101636

del Rio L, Marban G (2012) Stainless steel wire mesh-supported potassium-doped cobalt oxide catalysts for the catalytic decomposition of nitrous oxide. Appl Catal B 126:39–46. https://doi.org/10.1016/j.apcatb.2012.06.022

del Rio L, Lopez I, Marban G (2014) Stainless steel wire mesh-supported Co_3O_4 catalysts in the steam reforming of ethanol. Appl Catal B 150:370–379. https://doi.org/10.1016/j.apcatb.2013.12.022

du Preez SP, Jones DR, Bessarabov DG, Falch A, Quaresma CMD, Dunnill CW (2019) Development of a Pt/stainless steel mesh catalyst and its application in catalytic hydrogen combustion. Int J Hydrog Energy 44:27094–27106. https://doi.org/10.1016/j.ijhydene.2019.08.168

Duran FG, Barbero BP, Cadus LE (2011) Preparation of MnOx/AISI 304 Austenitic Stainless Steel Monoliths for Catalytic Combustion of Ethyl Acetate. Catal Letters 141:1786–1795. https://doi.org/10.1007/s10562-011-0716-x

Dvorakova M, Perekrestov R, Ksirova P, Balabanova J, Jiratova K, Maixner J, Topka P, Rathousky J, Kostejn M, Cada M, Hubicka Z, Kovanda F (2019) Preparation of cobalt oxide catalysts on stainless steel wire mesh by combination of magnetron sputtering and electrochemical deposition. Catal Today 334:13–23. https://doi.org/10.1016/j.cattod.2019.03.008

Falsafein M, Ashrafizadeh F, Kheirandish A (2018) Influence of thickness on adhesion of nanostructured multilayer CrN/CrAlN coatings to stainless steel substrate. Surf Interfaces 13:178–185. https://doi.org/10.1016/j.surfin.2018.09.009

Fu K, Su Y, Yang L, Ji N, Song C, Ma D, Lv X, Han R, Liu Q (2022) Pt loaded manganese oxide nanoarray-based monolithic catalysts for catalytic oxidation of acetone. Chem Eng J 432:134397. https://doi.org/10.1016/j.cej.2021.134397

Ganley JC, Riechmann KL, Seebauer EG, Masel RI (2004) Porous anodic alumina optimized as a catalyst support for microreactors. J Catal 227:26–32. https://doi.org/10.1016/j.jcat.2004.06.016

Garcia-Lobato MA, Mtz-Enriquez AI, Garcia CR, Velazquez-Manzanares M, Avalos-Belmontes F, Ramos-Gonzalez R, Garcia-Cerda LA (2019) Corrosion resistance and in vitro bioactivity of dense and porous titania coatings deposited on 316L SS by spraying method. Appl Surf Sci 484:975–980. https://doi.org/10.1016/j.apsusc.2019.04.108

Geng Y, Cao Y, Zhao Q, Li Y, Tian S (2022) Potential hazards associated with interactions between diesel exhaust particulate matter and pulmonary surfactant. Sci Total Environ 807:151031. https://doi.org/10.1016/j.scitotenv.2021.151031

Gholami F, Tomas M, Gholami Z, Vakili M (2020) Technologies for the nitrogen oxides reduction from flue gas: A review. Sci Total Environ 714:136712. https://doi.org/10.1016/j.scitotenv.2020.136712

Godoy ML, Banus ED, Sanz O, Montes M, Miro E, Milt VG (2018) Stacked Wire Mesh Monoliths for the Simultaneous Abatement of VOCs and Diesel Soot. Catalysts 8:16. https://doi.org/10.3390/catal8010016

Gómez MJ, Diaz LA, Franceschini EA, Lacconi GI, Abuin GC (2019) 3D nanostructured NiMo catalyst electrodeposited on 316L stainless steel for hydrogen generation in industrial applications. J Appl Electrochem 49:1227–1238. https://doi.org/10.1007/s10800-019-01361-8

Gómez MJ, Lucci RO, Franceschini EA, Lacconi GI (2021) Effect of TiO_2 content on Ni/TiO_2 composites electrodeposited on SS316L for hydrogen evolution reaction. Electrochim Acta 378:138136. https://doi.org/10.1016/j.electacta.2021.138136

Govender S, Friedrich HB (2017) Monoliths: A Review of the Basics, Preparation Methods and Their Relevance to Oxidation. Catalysts 7:29. https://doi.org/10.3390/catal7020062

Guo Y, Li HB, Kameyama H (2011a) Steam reforming of kerosene over a metal-monolithic alumina-supported Ru catalyst: Effect of preparation conditions and electrical-heating test. Chem Eng Sci 66:6287–6296. https://doi.org/10.1016/j.ces.2011.09.008

Guo Y, Zhou L, Kameyama H (2011b) Thermal and hydrothermal stability of a metal monolithic anodic alumina support for steam reforming of methane. Chem Eng J 168:341–350. https://doi.org/10.1016/j.cej.2011.01.036

He C, Cheng J, Zhang X, Douthwaite M, Pattisson S, Hao ZP (2019) Recent Advances in the Catalytic Oxidation of Volatile Organic Compounds: A Review Based on Pollutant Sorts and Sources. Chem Rev 119:4471–4568. https://doi.org/10.1021/acs.chemrev.8b00408

Health Effects Institute (2020). State of Global Air 2020. Special Report. Boston, MA:Health Effects Institute. https://www.stateofglobalair.org/

Ho PH, Jablonska M, Palkovits R, Rodriguez-Castellon E, Ospitali F, Fornasari G, Vaccari A, Benito P (2020) N_2O catalytic decomposition on electrodeposited Rh-based open-cell metallic foams. Chem Eng J 379:11. https://doi.org/10.1016/j.cej.2019.122259

Hoang AT (2021) Combustion behavior, performance and emission characteristics of diesel engine fuelled with biodiesel containing cerium oxide nanoparticles: A review. Fuel Process Technol 218:106840. https://doi.org/10.1016/j.fuproc.2021.106840

Honcharov V, Zazhigalov V, Sawlowicz Z, Socha R, Gurgol J (2016) Structural, Catalytic, and Thermal Properties of Stainless Steel with Nanoscale Metal Surface Layer, 4th International Research and Practice Conference on Nanotechnology and Nanomaterials (NANO). Springer Proceedings in Physics. Springer-Verlag Berlin, Lviv, UKRAINE, pp. 355–364

Hu JS, Wang BL (2021) Crack growth behavior and thermal shock resistance of ceramic sandwich structures with an auxetic honeycomb core. Compos Struct 260. https://doi.org/10.1016/j.compstruct.2020.113256

Huang Y, Wang JJ, Zou Y, Jiang LW, Liu XL, Jiang WJ, Liu H, Hu JS (2021) Selective Se doping of $NiFe_2O_4$ on an active NiOOH scaffold for efficient and robust water oxidation. Chinese J Catal 42:1395–1403. https://doi.org/10.1016/s1872-2067(20)63739-1

Jeong SB, Lee DU, Lee BJ, Heo KJ, Kim DW, Hwang GB, MacRobert AJ, Shin JH, Ko HS, Park SK, Oh YS, Kim SJ, Lee DY, Lee SB, Park I, Kim SB, Han B, Jung JH, Choi DY (2022) Photobiocidal-triboelectric nanolayer coating of photosensitizer/silica-alumina for reusable and visible-light-driven antibacterial/antiviral air filters. Chem Eng J 440:135830. https://doi.org/10.1016/j.cej.2022.135830

Karimi N, Riffard F, Rabaste F, Perrier S, Cueff R, Issartel C, Buscail H (2008) Characterization of the oxides formed at 1000 degrees C on the AISI 304 stainless steel by X-ray diffraction and infrared spectroscopy. Appl Surf Sci 254:2292–2299. https://doi.org/10.1016/j.apsusc.2007.09.018

Kavitha G, Vinoth Kumar J, Devanesan S, Asemi NN, Manikandan V, Arulmozhi R, Abirami N (2022) Ceria nanoparticles anchored on graphitic oxide sheets (CeO_2-GOS) as an efficient catalyst for degradation of dyes and textile effluents. Environ Res 209:112750. https://doi.org/10.1016/j.envres.2022.112750

Khan GR, Malik SI (2022) Ag-enriched TiO_2 nanocoating apposite for self-sanitizing/ self-sterilizing/ self-disinfecting of glass surfaces.

Mater Chem Phys 282:125803. https://doi.org/10.1016/j.matchemphys.2022.125803

Kim M-J, Kim Y-J, Lee S-J, Ryu I-S, Kim HJ, Kim Y, Ko CH, Jeon SG (2019) Enhanced catalytic activity of the Rh/γ-Al_2O_3 pellet catalyst for N_2O decomposition using high Rh dispersion induced by citric acid. Chem Eng Res Des 141:455–463. https://doi.org/10.1016/j.cherd.2018.11.016

Volodarskaja A, Kuśtrowski P, Rokicińska A, Fridrichová D, Obalová L (2019) Cobalt mixed oxides deposited on the SiC open-cell foams for nitrous oxide decomposition. Appl Catal B 255https://doi.org/10.1016/j.apcatb.2019.117745

Klyushina A, Pacultova K, Krejcova S, Slowik G, Jiratova K, Kovanda F, Ryczkowski J, Obalova L (2015) Advantages of stainless steel sieves as support for catalytic N_2O decomposition over K-doped Co_3O_4. Catal Today 257:2–10. https://doi.org/10.1016/j.cattod.2015.05.015

Koo KY, Eom HJ, Jung UH, Yoon WL (2016) Ni nanosheet-coated monolith catalyst with high performance for hydrogen production via natural gas steam reforming. Appl Catal A Gen 525:103–109. https://doi.org/10.1016/j.apcata.2016.07.016

Koo KY, Eom HJ, Kwon SC, Jung UH, Yoon WL (2017) Ru-coated metal monolith catalyst prepared by novel coating method for hydrogen production via natural gas steam reforming. Catal Today 293–294:129–135. https://doi.org/10.1016/j.cattod.2016.11.016

Kotter M, Riekert L, Weyland F (1983) Deposition of ternary oxides as active components by impregnation of porous carriers. Stud Surf Sci Catal 16:521–530. https://doi.org/10.1016/S0167-2991(09)60045-8

Kouotou PM, Pan GF, Weng JJ, Fan SB, Tian ZY (2016) Stainless steel grid mesh-supported CVD made Co_3O_4 thin films for catalytic oxidation of VOCs of olefins type at low temperature. J Ind Eng Chem 35:253–261. https://doi.org/10.1016/j.jiec.2015.12.039

Kucharczyk B, Tylus W, Okal J, Chęcmanowski J, Szczygieł B (2017) The Pt-NiO catalysts over the metallic monolithic support for oxidation of carbon monoxide and hexane. Chem Eng J 309:288–297. https://doi.org/10.1016/j.cej.2016.10.032

Labrecque R, Lavoie JM (2011) Dry reforming of methane with CO_2 on an electron-activated iron catalytic bed. Bioresour Technol 102:11244–11248. https://doi.org/10.1016/j.biortech.2011.09.088

Lee M, Jee MS, Lee SY, Cho MK, Ahn JP, Oh HS, Kim W, Hwang YJ, Min BK (2018) Sloughing a Precursor Layer to Expose Active Stainless Steel Catalyst for Water Oxidation. Acs Appl Mater Inter 10:24499–24507. https://doi.org/10.1021/acsami.8b04871

Li HQ, Chen M, Zheng XM (2003) A novel catalyst supported on stainless steel pretreated by anodic oxidation for control of volatile organic compound emissions. Chinese J Catal 24:807–808. https://doi.org/10.1016/S0301-0104(03)00390-2

Li JJ, Lu XF, Wu F, Cheng W, Zhang WD, Qin SL, Wang Z, You ZX (2017a) Electroplated Palladium Catalysts on FeCrAlloy for Joule-Heat-Ignited Catalytic Elimination of Ethylene in Air. Ind Eng Chem Res 56:12520–12528. https://doi.org/10.1021/acs.iecr.7b03044

Li JJ, Lu XF, Wu F, Qin SL, You ZX (2017b) Metallic-substrate-supported manganese oxide as Joule-heat-ignition catalytic reactor for removal of carbon monoxide and toluene in air. Chem Eng J 328:1058–1065. https://doi.org/10.1016/j.cej.2017.07.128

Li H, Wang Y, Chen X, Liu S, Zhou Y, Zhu QL, Chen YF, Lu HF (2018) Preparation of metallic monolithic Pt/FeCrAl fiber catalyst by suspension spraying for VOCs combustion. Rsc Adv 8:14806–14811. https://doi.org/10.1039/c8ra01720d

Li ZD, Chen L, Yang QC, Yang H, Zhou Y (2021) Compacted stainless steel mesh-supported Co_3O_4 porous nanobelts for HCHO catalytic oxidation and Co_3O_4@Co_3S_4 via in situ sulfurization as platinum-free counter electrode for flexible dye-sensitized solar cells. Appl Surf Sci 536:11. https://doi.org/10.1016/j.apsusc.2020.147815

Li X, Li Q, Li W, Zhang X, Zhong L, Zhang C, Fang Q, Chen G (2019) Enhancement of SCR performance of monolithic Mn–Ce/Al_2O_3/cordierite catalysts by using modified deposition precipitation method. Asia-Pacific J Chem Eng 14.https://doi.org/10.1002/apj.2318

Lin X, Li S, He H, Wu Z, Wu J, Chen L, Ye D, Fu M (2018) Evolution of oxygen vacancies in MnOx-CeO_2 mixed oxides for soot oxidation. Appl Catal B 223:91–102. https://doi.org/10.1016/j.apcatb.2017.06.071

Ling C, Gao YY, Li XX, Chen M (2013) The preparation of ZSM-5 zeolite@Cu/stainless steel as a dual functional material. J Porous Mat 20:839–844. https://doi.org/10.1007/s10934-012-9659-x

Liu J, Kang L, Li H, Maitarad P, Zhang J, Shi L, Zhang D (2017) Mn–Fe bi-metal oxides in situ created on metal wire mesh as monolith catalysts for selective catalytic reduction of NO with NH_3. Rsc Adv 7:40444–40451. https://doi.org/10.1039/c7ra05007k

Liu YH, Zhang KW, Zhang DX, Dong WX, Jiang TY, Zhou HB, Li LX, Mao BD (2021) Industrial stainless steel meshes for efficient electrocatalytic hydrogen evolution. J Energy Storage 41:7. https://doi.org/10.1016/j.est.2021.102844

Luo C, Fan SS, Li G, Lang XM (2019) Catalytic combustion of methyl ethyl ketone over paper-like microfibrous entrapped MnOx/AC catalyst. Mater Chem Phys 230:17–24. https://doi.org/10.1016/j.matchemphys.2019.03.036

Ma Y, Chen M, Song C, Zheng X (2008) Catalytic Oxidation of Toluene, Acetone and Ethyl Acetate on a New Pt-Pd/Stainless Steel Wire Mesh Catalyst. Acta Phys-Chim Sin 24:1132–1136. https://doi.org/10.1016/S1872-1508(08)60047-9

Ma M, Yang R, He C, Jiang Z, Shi J-W, Albilali R, Fayaz K, Liu B (2021) Pd-based catalysts promoted by hierarchical porous Al_2O_3 and ZnO microsphere supports/coatings for ethyl acetate highly active and stable destruction. J Hazard Mater 401:123281. https://doi.org/10.1016/j.jhazmat.2020.123281

Marban G, Lopez A, Lopez I, Valdes-Solis T (2010) A highly active, selective and stable copper/cobalt-structured nanocatalyst for methanol decomposition. Appl Catal B 99:257–264. https://doi.org/10.1016/j.apcatb.2010.06.028

Martinez LM, Sanz O, Dominguez MI, Centeno MA, Odriozola JA (2009) AISI 304 Austenitic stainless steels monoliths for catalytic applications. Chem Eng J 148:191–200. https://doi.org/10.1016/j.cej.2008.12.030

Mei XY, Zhu XB, Zhang YX, Zhang ZL, Zhong ZC, Xin Y, Zhang J (2021) Decreasing the catalytic ignition temperature of diesel soot using electrified conductive oxide catalysts. Nat Catal 4:1002–1011. https://doi.org/10.1038/s41929-021-00702-1

Meille V (2006) Review on methods to deposit catalysts on structured surfaces. Appl Catal A Gen 315:1–17. https://doi.org/10.1016/j.apcata.2006.08.031

Mo S, Zhang Q, Li J, Sun Y, Ren Q, Zou S, Zhang Q, Lu J, Fu M, Mo D, Wu J, Huang H, Ye D (2020) Highly efficient mesoporous MnO_2 catalysts for the total toluene oxidation: Oxygen-Vacancy defect engineering and involved intermediates using in situ DRIFTS. Appl Catal B 264:118464. https://doi.org/10.1016/j.apcatb.2019.118464

Montebelli A, Visconti CG, Groppi G, Tronconi E, Cristiani C, Ferreira C, Kohler S (2014) Methods for the catalytic activation of metallic structured substrates. Catal Sci Technol 4:2846–2870. https://doi.org/10.1039/c4cy00179f

Nady H, El-Rabiei MM, Samy M, Deyab MA, Abd El-Hafez GM (2021) Novel Ni–Cr-based alloys as hydrogen fuel sources through alkaline water electrolytes. Int J Hydrogen Energ 46:34749–34766. https://doi.org/10.1016/j.ijhydene.2021.08.056

Ni SQ, Tang XL, Yi HH, Gao FY, Wang CZ, Shi YR, Zhang RC, Zhu WJ (2022) Novel Mn-Ce bi-oxides loaded on 3D monolithic

nickel foam for low-temperature NH_3-SCR de-NOx: Preparation optimization and reaction mechanism. J Rare Earths 40:268–278. https://doi.org/10.1016/j.jre.2020.12.015

Nikolaieva DY, Honcharov VV, Ivashin DY, Zazhigalov VO (2021) Use of Spectroscopy and Computer Simulation to the Study of Surfaces Modified by Ionic Implantation. Ukr J Phys 66. https://doi.org/10.15407/ujpe66.6.511

Padilha AF, Plaut RL, Rios PR (2006) Stainless steel heat treatment, Steel Heat Treatment: Metallurgy and Technologies, pp. 695–739

Pauletto G, Vaccari A, Groppi G, Bricaud L, Benito P, Boffito DC, Lercher JA, Patience GS (2020) FeCrAl as a Catalyst Support. Chem Rev 120:7516–7550. https://doi.org/10.1021/acs.chemrev.0c00149

Pauletto G, Libretto N, Boffito DC, Miller JT, Jentys A, Patience GS, Lercher JA (2021a) Ni/CeO_2 promoted Ru and Pt supported on FeCrAl gauze for cycling methane catalytic partial oxidation-CPDX. Appl Catal B 286:8. https://doi.org/10.1016/j.apcatb.2020.119849

Pauletto G, Mendil M, Libretto N, Mocellin P, Miller JT, Patience GS (2021b) Short contact time CH4 partial oxidation over Ni based catalyst at 1.5 MPa. Chem Eng J 414:9. https://doi.org/10.1016/j.cej.2021b.128831

Pecchi G, Reyes P (2003) Catalytic activity of sol-gel metal and metal oxide catalysts, Emerging Fields in So-gel Science and Technology, pp. 24–36

Peng C, Yu D, Zhang C, Chen M, Wang L, Yu X, Fan X, Zhao Z, Cheng K, Chen Y, Wei Y, Liu J (2023) Alkali/alkaline-earth metal-modified MnOx supported on three-dimensionally ordered macroporous–mesoporous $Ti_xSi_{1-x}O_2$ catalysts: Preparation and catalytic performance for soot combustion. J Environ Sci-China 125:82–94. https://doi.org/10.1016/j.jes.2021.10.029

Porsin AV, Kulikov AV, Rogozhnikov VN, Serkova AN, Salanov AN, Shefer KI (2016) Structured reactors on a metal mesh catalyst for various applications. Catal Today 273:213–220. https://doi.org/10.1016/j.cattod.2016.03.033

Qi GL, Zhang YX, Chen AB, Yu YF (2017) Potassium-Activated Wire Mesh: A Stable Monolithic Catalyst for Diesel Soot Combustion. Chem Eng Technol 40:50–55. https://doi.org/10.1002/ceat.201600137

Qu ZP, Wang Z, Quan X, Wang H, Shu Y (2013) Selective catalytic oxidation of ammonia to N_2 over wire-mesh honeycomb catalyst in simulated synthetic ammonia stream. Chem Eng J 233:233–241. https://doi.org/10.1016/j.cej.2013.08.028

Rieks M, Bellinghausen R, Kockmann N, Mleczko L (2015) Experimental study of methane dry reforming in an electrically heated reactor. Int J of Hydrog Energy 40:15940–15951. https://doi.org/10.1016/j.ijhydene.2015.09.113

Rogozhnikov VN, Salanov AN, Potemkin DI, Pakharukova VP, Stonkus OA, Glotov AP, Boev SS, Zasypalov GO, Melnikov DP, Snytnikov PV (2022) Structured composite catalyst Pd/$Ce_{0.75}Zr_{0.25}O_{2-x}$/θ-$Al_2O_3$/FeCrAlloy for complete oxidation of methane. Mater Lett 310. https://doi.org/10.1016/j.matlet.2021.131481

Saeki I, Konno H, Furuichi R, Nakamura T, Mabuchi K, Itoh M (1998) The effect of the oxidation atmosphere on the initial oxidation of type 430 stainless steel at 1273 K. Corros Sci 40:191–200. https://doi.org/10.1016/S0010-938X(97)00113-3

Santos DFM, Soares O, Figueiredo JL, Sanz O, Montes M, Pereira MFR (2020) Preparation of ceramic and metallic monoliths coated with cryptomelane as catalysts for VOC abatement. Chem Eng J 382:9. https://doi.org/10.1016/j.cej.2019.122923

Sanz O, Velasco I, Reyero I, Legorburu I, Arzamendi G, Gandia LM, Montes M (2016) Effect of the thermal conductivity of metallic monoliths on methanol steam reforming. Catal Today 273:131–139. https://doi.org/10.1016/j.cattod.2016.03.008

Sanz O, Banus ED, Goya A, Larumbe H, Delgado JJ, Monzon A, Montes M (2017) Stacked wire-mesh monoliths for VOCs combustion: Effect of the mesh-opening in the catalytic performance. Catal Today 296:76–83. https://doi.org/10.1016/j.cattod.2017.05.054

Sanzhak O, Goncharov V, Azimov F, Brazhnyk D, Zazhigalov V (2018) Preparation of new photocatalytic materials using ion implantation method. Mol Cryst Liq Cryst 671:156–163. https://doi.org/10.1080/15421406.2018.1542098

Schafer H, Chatenet M (2018) Steel: The Resurrection of a Forgotten Water-Splitting Catalyst. Acs Energy Lett 3:574–591. https://doi.org/10.1021/acsenergylett.8b00024

Serrano EB, Oropeza-Guzmán MT, López-Maldonado EA (2018) Innovation in the Electrophoretic Deposition of TiO_2 Using Different Stabilizing Agents and Zeta Potential, Titanium Dioxide - Material for a Sustainable Environment

Shen JY, Wang M, Zhao L, Jiang J, Liu H, Liu JX (2018) Self-Supported Stainless Steel Nanocone Array Coated with a Layer of Ni-Fe Oxides/(Oxy)hydroxides as a Highly Active and Robust Electrode for Water Oxidation. Acs Appl Mater Inter 10:8786–8796. https://doi.org/10.1021/acsami.8b00498

Shu Y, Sun H, Quan X, Chen S (2012a) Improvement of Water-, Sulfur Dioxide-, and Dust-Resistance in Selective Catalytic Reduction of NOx with NH_3 Using a Wire-Mesh Honeycomb Catalyst. Ind Eng Chem Res 51:7867–7873. https://doi.org/10.1021/ie300832d

Shu Y, Sun H, Quan X, Chen SO (2012b) Enhancement of Catalytic Activity Over the Iron-Modified Ce/TiO_2 Catalyst for Selective Catalytic Reduction of NOx with Ammonia. J Phys Chem C 116:25319–25327. https://doi.org/10.1021/jp307038q

Shu Y, Aikebaier T, Quan X, Chen S, Yu HT (2014) Selective catalytic reaction of NOx with NH_3 over Ce-Fe/TiO_2-loaded wire-mesh honeycomb: Resistance to SO_2 poisoning. Appl Catal B 150:630–635. https://doi.org/10.1016/j.apcatb.2014.01.008

Singh TS, Rajak U, Verma TN, Nashine P, Mehboob H, Manokar AM, Afzal A (2022) Exhaust emission characteristics study of light and heavy-duty diesel vehicles in India. Case Stud Therm Eng 29:101709. https://doi.org/10.1016/j.csite.2021.101709

Song C, Chen M, Ma Ca, Zheng X (2009) Pd-Mn/Stainless Steel Wire Mesh Catalyst for Catalytic Oxidation of Toluene, Acetone and Ethyl Acetate. Chinese J of Chem 27(10):1903–1906. https://doi.org/10.1002/cjoc.200990319

Su CS, McGinn PJ (2014) Application of glass soot catalysts on metal supports to achieve low soot oxidation temperature. Catal Commun 43:1–5. https://doi.org/10.1016/j.catcom.2013.08.013

Suknev A, van Veen AC, Toktarev A, Sadovskaya E, Bal'zhinimaev B, Mirodatos C (2004) NO decomposition over a new type of low metal content fiberglass catalysts studied by the TAP technique. Catal Commun 5:691–695. https://doi.org/10.1016/j.catcom.2004.08.009

Sun H, Quan X, Zhang Y-b, Zhao Y-z (2008a) Selective catalytic reduction of NOx over Pd/CeZr/TiO_2/Al_2O_3 wire-mesh honeycomb catalysts. Environ Sci 29:1743–1748. https://doi.org/10.13227/j.hjkx.2008.06.005

Sun H, Zhang YB, Quan X, Chen S, Qu ZP, Zhou YL (2008b) Wire-mesh honeycomb catalyst for selective catalytic reduction of NOx under lean-burn conditions. Catal Today 139:130–134. https://doi.org/10.1016/j.cattod.2008.08.021

Sun H, Shu Y, Quan X, Chen S, Pang B, Liu Z (2010) Experimental and modeling study of selective catalytic reduction of NOx with NH_3 over wire mesh honeycomb catalysts. Chem Eng J 165:769–775. https://doi.org/10.1016/j.cej.2010.09.057

Sun L, Xu RD, He SW, Wu TY (2021) A novel Co_3O_4 and WC co-doped β-PbO_2 electrode for zinc electrowinning: Deposition behavior and electrochemical properties. Acta Materiae Compositae Sinica 38:557–571. https://doi.org/10.13801/j.cnki.fhclxb.20200610.006

Topka P, Jiratova K, Dvorakova M, Balabanova J, Kostejn M, Kovanda F (2022) Hydrothermal deposition as a novel method for the preparation of Co-Mn mixed oxide catalysts supported on stainless steel meshes: application to VOC oxidation. Environ Sci Pollut R 29:5172–5183. https://doi.org/10.1007/s11356-021-15906-y

UNEP (2021) Actions on Air Quality: A Global Summary of Policies and Programmes to Reduce Air Pollution. https://wedocs.unep.org/20.500.11822/7677

Visconti CG, Groppi G, Tronconi E (2013) Accurate prediction of the effective radial conductivity of highly conductive honeycomb monoliths with square channels. Chem Eng J 223:224–230. https://doi.org/10.1016/j.cej.2013.02.095

Vorob'eva MP, Greish AA, Ivanov AV, Kustov LM (2000) Preparation of catalyst carriers on the basis of alumina supported on metallic gauzes. Appl Catal A Gen 199:257–261. https://doi.org/10.1016/s0926-860x(99)00563-3

Wang Y, Sui L, Kang H, Yu L (2018) Research on K-V-rare Earth Metal Catalysts for Diesel Soot Oxidation. Journal of Wuhan University of Technology-Mater. Sci Ed 33:331–337. https://doi.org/10.1007/s11595-018-1825-8

Wang J, Zhang Y, Kuang L, Yang J, Xu C, Mu B, Li J, Lu P, Song W, Wang W, Wu A, Liang X, Zhang J (2021) Low-voltage driven Ag-Co_3O_4 textile device for multifunctional air cleaning. Chem Eng J 424.https://doi.org/10.1016/j.cej.2021.130320

Wang Y, Xu W, Chen X, Li C, Xie J, Yang Y, Zhu T, Zhang C (2022a) Single–atom Ir_1 supported on rutile TiO_2 for excellent selective catalytic oxidation of ammonia. J Hazard Mater 432.https://doi.org/10.1016/j.jhazmat.2022a.128670

Wang Y, Xu W, Li C, Yang Y, Geng Z, Zhu T (2022b) Effects of IrO_2 nanoparticle sizes on Ir/Al_2O_3 catalysts for the selective catalytic oxidation of ammonia. Chem Eng J 437.https://doi.org/10.1016/j.cej.2022b.135398

Wu XD, Weng D, Chen Z, Xu LH (2001) Effects of plasma-sprayed NiCrAl/ZrO_2 intermediate on the combination ability of coatings. Surf Coat Technol 140:231–237. https://doi.org/10.1016/s0257-8972(01)01166-5

Wu XD, Weng D, Zhao S, Chen W (2005) Influence of an aluminized intermediate layer on the adhesion of a gamma-Al_2O_3 washcoat on FeCrAl. Surf Coat Technol 190:434–439. https://doi.org/10.1016/j.surfcoat.2004.03.007

Wu DF, Zhang YH, Li YD (2017) Mechanical stability of monolithic catalysts: Improving washcoat adhesion by FeCrAl alloy substrate treatment. J Ind Eng Chem 56:175–184. https://doi.org/10.1016/j.jiec.2017.07.010

Wunsch R, Fichtner M, Gorke O, Haas-Santo K, Schubert K (2002) Process of applying Al_2O_3 coatings in microchannels of completely manufactured microstructured reactors. Chem Eng Technol 25:700–703. https://doi.org/10.1002/1521-4125(20020709)25:7%3c700::Aid-ceat700%3e3.0.Co;2-i

Xia YT, Wang JL, Gu CQ, Ling Y, Gao ZM (2020) MnO_2/Al foil decorated air cleaner with self-driven property for the abatement of indoor formaldehyde. Chem Eng J 382:8. https://doi.org/10.1016/j.cej.2019.122872

Xin BW, Sun GW, Lao CF, Shang DH, Zhang XY, Wen ZJ, He MS (2019) Chemical vapor deposition synthesis of carbon nanosprouts on calcined stainless steel. Mater Lett 238:290–293. https://doi.org/10.1016/j.matlet.2018.12.019

Xue TS, Li RN, Gao YS, Wang Q (2020) Iron mesh-supported vertically aligned Co-Fe layered double oxide as a novel monolithic catalyst for catalytic oxidation of toluene. Chem Eng J 384:11. https://doi.org/10.1016/j.cej.2019.123284

Yan Y, Wang Z, Ding T, Zhang H (2022) Preparation and application of Co_3O_4 catalysts from ZIF-67 membranes over paper-like stainless steel fibers in isopropanol combustion. J Solid State Chem 308.https://doi.org/10.1016/j.jssc.2022.122880

Yang KS, Jiang Z, Shik Chung J (2003) Electrophoretically Al-coated wire mesh and its application for catalytic oxidation of 1,2-dichlorobenzene. Surf Coat Tech 168:103–110. https://doi.org/10.1016/S0257-8972(02)00569-8

Yang KS, Choi JS, Chung JS (2004a) Evaluation of wire-mesh honeycomb containing porous Al/Al_2O_3 layer for catalytic combustion of ethyl acetate in air. Catal Today 97:159–165. https://doi.org/10.1016/j.cattod.2004.04.057

Yang KS, Choi JS, Lee SH, Chung JS (2004b) Development of Al/Al_2O_3-coated wire-mesh honeycombs for catalytic combustion of volatile organic compounds in air. Ind Eng Chem Res 43:907–912. https://doi.org/10.1021/ie034022g

Yang KS, Mul G, Choi JS, Moulijn JA, Chung JS (2006) Development of TiO_2/Ti wire-mesh honeycomb for catalytic combustion of ethyl acetate in air. Appl Catal AGen 313:86–93. https://doi.org/10.1016/j.apcata.2006.07.008

Yao J, Choi JS, Yang KS, Sun DZ, Chung JS (2006) Wire-mesh honeycomb catalysts for selective catalytic reduction of NO with NH_3. Korean J Chem Eng 23:888–895. https://doi.org/10.1007/s11814-006-0004-4

Yao H, Cai S, Yang B, Han L, Wang P, Li H, Yan T, Shi L, Zhang D (2020) In situ decorated MOF-derived Mn–Fe oxides on Fe mesh as novel monolithic catalysts for NOx reduction. New J Chem 44:2357–2366. https://doi.org/10.1039/c9nj05960a

Yao J, Dong F, Feng H, Tang Z (2022) Construction of superhydrophobic layer for enhancing the water-resistant performance of VOCs catalytic combustion. Fuel 314.https://doi.org/10.1016/j.fuel.2022.123139

Yin K, Zhang H, Yan Y (2019) High efficiency of toluene adsorption over a novel ZIF-67 membrane coating on paper-like stainless steel fibers. J Solid State Chem 279.https://doi.org/10.1016/j.jssc.2019.120976

Yu J, Ji G, Liu Q, Zhang J, Shi Z (2017) Effect of sol-gel ZrO_2 films on corrosion behavior of the 304 stainless steel in coal-gases environment at high temperature. Surf Coat Technol 331:21–26. https://doi.org/10.1016/j.surfcoat.2017.10.037

Yu D, Ren Y, Yu X, Fan X, Wang L, Wang R, Zhao Z, Cheng K, Chen Y, Sojka Z, Kotarba A, Wei Y, Liu J (2021a) Facile synthesis of birnessite-type $K_2Mn_4O_8$ and cryptomelane-type $K_{2-x}Mn_8O_{16}$ catalysts and their excellent catalytic performance for soot combustion with high resistance to H_2O and SO_2. Appl Catal B 285:119779. https://doi.org/10.1016/j.apcatb.2020.119779

Yu Y, Tan W, An D, Wang X, Liu A, Zou W, Tang C, Ge C, Tong Q, Sun J, Dong L (2021b) Insight into the SO_2 resistance mechanism on γ-Fe_2O_3 catalyst in 3-SCR reaction: A collaborated experimental and DFT study. Appl Catal B 281:119544. https://doi.org/10.1016/j.apcatb.2020.119544

Yuan B, Chen H, Zhao R, Deng X, Chen G, Yang X, Xiao Z, Aurora A, Iulia BA, Zhang K, Zhu X, Iulian AV, Hai S, Zhang X (2022) Construction of a magnesium hydroxide/graphene oxide/hydroxyapatite composite coating on Mg-Ca-Zn-Ag alloy to inhibit bacterial infection and promote bone regeneration. Bioact Mater 18:354–367. https://doi.org/10.1016/j.bioactmat.2022.02.030

Zazhigalov SV, Shilov VA, Rogozhnikov VN, Potemkin DI, Sobyanin VA, Zagoruiko AN, Snytnikov PV (2021) Modeling of hydrogen production by diesel reforming over Rh/$Ce_{0.75}Zr_{0.25}O_2$-delta-eta-Al_2O_3/FeCrAl wire mesh honeycomb catalytic module. Catal Today 378:240–248. https://doi.org/10.1016/j.cattod.2020.11.015

Zha KW, Sun WJ, Huang Z, Xu HL, Shen W (2020) Insights into High-Performance Monolith Catalysts of Co_3O_4 Nanowires Grown on Nickel Foam with Abundant Oxygen Vacancies for Formaldehyde Oxidation. Acs Catal 10:12127–12138. https://doi.org/10.1021/acscatal.0c02944

Zhang T, Chen M, Gao YY, Zheng XM (2010) 0.1%Pt-0.02%Pd/Stainless Steel Monolith Catalyst: Catalytic Oxidation of Acetone and Thermal Stability. Chinese J Inorg Chem 26:1370–1374. https://doi.org/10.1016/j.poly.2010.05.029

Zhang T, Chen M, Gao Y-y, Zheng X-m (2012) Preparation process and characterization of new Pt/stainless steel wire mesh catalyst designed for volatile organic compounds elimination. J Cent South Univ 19:319–323. https://doi.org/10.1007/s11771-012-1007-4

Zhang X, Xuan Y, Wang B, Gao C, Niu S, Zhao G, Wang D, Li J, Lu C, Crittenden JC (2022a) Precise regulation of acid pretreatment for red mud SCR catalyst: Targeting on optimizing the acidity and reducibility. Front Environ Sci Eng 16:88–98. https://doi.org/10.1007/s11783-021-1447-x

Zhang Y, Zhang Y, Wu C, Yang Y, Li Q, Chen Y (2022b) Oxidation behavior and electrical properties of metal interconnects with Ce-doped Ni–Mn spinel coatings. Ceram Int 48:9550–9557. https://doi.org/10.1016/j.ceramint.2021.12.153

Zhang Y, Zhang H, Yan Y (2020) Kinetic studies of trichloroethylene catalytic combustion over Cr/ZSM-5/PSSF composite. Sep Purif Technol 251.https://doi.org/10.1016/j.seppur.2020.116827

Zhao L, Zhang Z, Li Y, Leng X, Zhang T, Yuan F, Niu X, Zhu Y (2019) Synthesis of CeaMnOx hollow microsphere with hierarchical structure and its excellent catalytic performance for toluene combustion. Appl Catal B 245:502–512. https://doi.org/10.1016/j.apcatb.2019.01.005

Zhao Q, Zheng YF, Song CF, Liu QL, Ji N, Ma DG, Lu XB (2020) Novel monolithic catalysts derived from in-situ decoration of Co_3O_4 and hierarchical Co_3O_4@MnOx on Ni foam for VOC oxidation. Appl Catal B 265:12. https://doi.org/10.1016/j.apcatb.2019.118552

Zhong CT, Xiong XP (2021) Preparation of a composite coating film via vapor induced phase separation for air purification and real-time bacteria photocatalytic inactivation. Prog Org Coat 161:8. https://doi.org/10.1016/j.porgcoat.2021.106486

Zhou L, Guo Y, Zhang Q, Yagi M, Hatakeyama J, Li HB, Chen J, Sakurai M, Kameyama H (2008) A novel catalyst with plate-type anodic alumina supports, Ni/$NiAl_2O_4$/gamma-Al_2O_3/alloy, for steam reforming of methane. Appl Catal A Gen 347:200–207. https://doi.org/10.1016/j.apcata.2008.06.007

Zhou CY, Zhang HP, Yan Y, Zhang XY (2017) Catalytic combustion of acetone over Cu/LTA zeolite membrane coated on stainless steel fibers by chemical vapor deposition. Micropor Mesopor Mat 248:139–148. https://doi.org/10.1016/j.micromeso.2017.04.020

Zhou Y, Zhang H, Yan Y (2020) Catalytic oxidation of ethyl acetate over CuO/ZSM-5 zeolite membrane coated on stainless steel fibers by chemical vapor deposition. Chem Eng Res Des 157:13–24. https://doi.org/10.1016/j.cherd.2020.02.026

Zhu JQ, Wang ZC, Dai HJ, Wang QQ, Yang R, Yu H, Liao MZ, Zhang J, Chen W, Wei Z, Li N, Du LJ, Shi DX, Wang WL, Zhang LX, Jiang Y, Zhang GY (2019a) Boundary activated hydrogen evolution reaction on monolayer MoS_2. Nat Commun 10:7. https://doi.org/10.1038/s41467-019-09269-9

Zhu QL, Li H, Wang Y, Zhou Y, Zhu AM, Chen X, Li XN, Chen YF, Lu HF (2019b) Novel metallic electrically heated monolithic catalysts towards VOC combustion. Catal Sci Technol 9:6638–6646. https://doi.org/10.1039/c9cy01477b

Zhu SL, Duan GY, Chang CP, Chen YM, Sun YZ, Tang Y, Wan PY, Pan JQ (2020) Fast Electrodeposited Nickle-Iron Hydroxide Nanosheets on Sintered Stainless Steel Felt as Bifunctional Electrocatalyts for Overall Water Splitting. Acs Sustain Chem Eng 8:9885–9895. https://doi.org/10.1021/acssuschemeng.0c03017

Zokoe J, Su C, McGinn PJ (2019) Soot Combustion Activity and Potassium Mobility in Diesel Particulate Filters Coated with a K-Ca–Si–O Glass Catalyst. Ind Eng Chem Res 58:11891–11901. https://doi.org/10.1021/acs.iecr.9b02381